Joint Impact of I/Q Imbalance and Imperfect CSI on SM-MIMO Systems Over Generalized Beckmann Fading Channels: Optimal Detection and Cramer-Rao Bound

Ayse Elif Canbilen, Salama Said Ikki, *Senior Member, IEEE*, Ertugrul Basar, *Senior Member, IEEE*, Seyfettin Sinan Gultekin, and Ibrahim Develi

***Abstract*— Spatial modulation (SM) has been shown to be a promising low-complexity alternative to the state-of-art multiple-input multiple-output (MIMO) schemes due to its novel transmission approach. This paper investigates the performance of SM-MIMO systems in the presence of two practical undesirable effects, namely in-phase (I) and quadrature-phase (Q) imbalance (IQI) and imperfect channel state information (ICSI). An optimum maximum likelihood detection (MLD) method is proposed to tackle the effects of self-interference and signal distortion caused by IQI impairment by adapting the traditional MLD technique in accordance with the asymmetric characteristics of the IQI. More particularly, upper-bounds of the closed-form average pairwise error probability (APEP) and the average bit error rate (ABER) are derived for generalized Beckmann fading channels. As erroneously interpreted channel coefficients at the receiver (Rx) cause the error rate to increase and the detection to fall short, Cramer-Rao bound, which is a lower bound on the variance of the channel estimator, is utilized to assess the estimation accuracy. The system performance is evaluated by analytical derivations that are corroborated with computer simulations. The obtained results show that ICSI and IQI should be seriously considered while designing the future SM-based wireless communication systems.**

***Index Terms*— Cramer-Rao bound, generalized Beckmann fading, I/Q imbalance, optimal ML detection, spatial modulation.**

Manuscript received May 14, 2019; revised September 12, 2019 and December 9, 2019; accepted January 13, 2020. Date of publication February 6, 2020; date of current version May 8, 2020. This work was supported by the Scientific and Technological Research Council of Turkey (TUBITAK) BIDEB-2214 International Doctoral Research Fellowship Programme. The work of Ertugrul Basar was supported by the Scientific and Technological Research Council of Turkey (TUBITAK) under Grant 218E035. The associate editor coordinating the review of this article and approving it for publication was R. He. *(Corresponding author: Ayse Elif Canbilen.)*

Ayse Elif Canbilen and Seyfettin Sinan Gultekin are with the Electrical and Electronics Engineering Department, Konya Technical University, 42250 Konya, Turkey (e-mail: aecanbilen@ktun.edu.tr; ssgultekin@ktun.edu.tr).

Salama Said Ikki is with the Department of Electrical Engineering, Lakehead University, Thunder Bay, ON P7B 5E1, Canada (e-mail: sikki@lakeheadu.ca).

Ertugrul Basar is with the Communications Research and Innovation Laboratory (CORELAB), Department of Electrical and Electronics Engineering, Koç University, 34450, Istanbul, Turkey (e-mail: ebasar@ku.edu.tr).

Ibrahim Develi is with the Department of Electrical and Electronics Engineering, Erciyes University, 38039 Kayseri, Turkey (e-mail: develi@erciyes.edu.tr).

Color versions of one or more of the figures in this article are available online at http://ieeexplore.ieee.org.

Digital Object Identifier 10.1109/TWC.2020.2970002

I. INTRODUCTION

THE 5th generation (5G) and beyond of wireless networks are expected not only to provide enormous bandwidth and ultrahigh data rates with considerably lower latency (less than 1 millisecond), but also enable a variety of new applications such as Internet of Things (IoT), humanoid robots and connected autonomous cars [1]. The report of the International Telecommunications Union (ITU) on the minimum requirements for International Mobile Telecommunications-2020 (IMT-2020) specifies a downlink peak data rate of 20 Gbps and a bandwith of at least 100 MHz [2]. Hence, novel physical layer (PHY) techniques are required to meet the demands of 5G and beyond. Although some effective PHY solutions such as millimeterwave (mmWave) communications, massive multiple-input multiple-output (MIMO) systems and flexible waveform designs have already been proposed, researchers are still interested in exploring innovative ways to convey information instead of traditional methods [3].

Index modulation (IM) techniques, which utilize the indices of the building blocks (e.g., transmit antennas, subcarriers, radio frequency (RF) mirrors, transmit light emitting diodes (LEDs), and so on) of the corresponding communication systems to transmit additional information bits, seem to be competitive candidates for next-generation wireless networks due to the advantages they promise in terms of spectral and energy efficiency as well as hardware simplicity [3], [4]. Introducing spatial modulation (SM), a member of the IM family, hence opened a door for alternative radical digital modulation schemes.

SM has been proposed as a novel transmission technique and uses transmitter (Tx) antenna indices as extra information sources for low-complexity and power-efficient applications of MIMO wireless systems [5]. In particular, it has been shown that SM is an excellent solution for main drawbacks of MIMO systems, including inter-channel interference (ICI), inter-antenna synchronization, and multiple RF chains at the Tx [6]. The basic idea of SM is to map a block of information bits into two units: i) a symbol chosen from a complex signal constellation diagram, and ii) a unique Tx-antenna index chosen from the set of a Tx-antenna array. This simple yet effective encoding mechanism provides a one-to-one

mapping between blocks of information bits to be transmitted and the spatial positions of the Tx-antennas in the antenna array [6], [7].

Hence, SM takes advantage of the location-specific characteristic of the wireless channel, i.e., the uniqueness of each Tx-Rx wireless link, for transmission [8]. It is known that SM can achieve better performance than traditional modulation schemes when the Rx has perfect channel state information (CSI) [9], [10]. A comprehensive survey on the SM system design and history was presented in [11] and [12]. Although SM is a promising technique for next-generation communication systems [13], [14], research in this field is still in its infancy and fundamental issues still need to be addressed to assess the possible applications of this technology in practical scenarios.

A. Related Works

The performance of SM-based MIMO systems has been extensively studied in the literature over Rayleigh, Rician, and Nakagami fading channels [15]–[17]. A comprehensive framework for the analysis of SM-MIMO over generalized fading channels was proposed in [18]. An analytical approach to the performance of SM and its simplified version, namely space shift keying (SSK), over Rayleigh flat fading channels in the presence of channel estimation error was developed in [19] and [20], respectively. An exact and closed-form expression of the average pairwise error probability (APEP) of SM and SSK over generalized $\alpha-\mu$ and $\kappa-\mu$ fading channels under the effect of imperfect CSI (ICSI) was derived in [21] and [22], respectively.

Although all aforementioned works assume ideal transceiver hardware, physical transceivers are affected by hardware impairments, such as phase noise and I/Q imbalance (IQI), that create distortions which degrade the performance of the communication systems [23]. For IoT and wearable devices, the IQI will be even more influential due to the use of cost-constrained analog components, such as mixers and phase shifters in their RF front-ends [24]. A dual-hop amplify-and-forward (AF) relaying system in the presence of IQI was analyzed and the destructive effects of IQI were addressed via maximum likelihood (ML) detection-based methods in [25]. The performance of underlay cognitive radio networks, which consider the effect of IQI, was studied in [26], and it was shown that the distorting effects of IQI is maximized in the case of ICSI.

On the other hand, SM becomes more attractive to be used against IQI effects as it outperforms single-input multiple-output (SIMO) systems with IQI [24]. Considering this, the effect of IQI on SM-based MIMO transmission was discussed in [27], and it was observed that both amplitude and phase IQI cause performance degradation for SM-based transmission. An optimal ML detector (MLD) was proposed and compared with a non-optimal Rx over Rayleigh fading channels in [28]. The joint impact of hardware imperfections and co-channel interference (CCI) on SSK-MIMO systems was investigated, and a closed-form expression of average BER (ABER) was derived for Rayleigh channels in [29].

The performance of pilot-aided estimation and data detection for MIMO systems was firstly investigated in [30], and Cramer-Rao lower bound (CRLB), which is a performance criterion that gives a lower bound to the mean square error of estimation in the set of unbiased estimates, was compared for different pilot insertion schemes. Then, the principle of CRLB was adapted for SM-based systems, and in order to assess the channel estimation accuracy, CRLB was computed for cognitive SM-MIMO systems with channel imperfections over Rayleigh fading channels in [31].

B. Motivation

It is an undeniable fact that estimation errors have destructive effects on the performance of wireless communication systems, including SM-based models [32]. Whether or not SM is more sensitive to channel imperfections than conventional systems has been a topic frequently discussed, since correct reception depends entirely on the uniqueness of channel coefficients and wrong estimation of CSI at Rx causes a BER increment [33], [34]. The studies in literature of SM-MIMO that considers ICSI either did not take into account the effect of any hardware impairments [21], [22], or only realized over Rayleigh fading channels [20], [31], [33], [34].

The generalized Beckmann distribution is a versatile multipath fading model that includes Rayleigh, Ricean, Beckmann, Hoyt (also known as Nakagami-q), single-sided Gaussian, $\kappa-\mu$ and Beaulieu-Xie distributions as special cases [35], [36]. Unlike other state-of-the-art envelope fading models, the impact of imbalances in the line-of-sight (LOS) and non-LOS (NLOS) components is considered simultaneously in generalized Beckmann fading [37]. Hence, this model effectively captures the correlation between the amplitude and phase [37]. It has a wide range of applications in RF communications, underwater wireless optical communications and free-space optical (FSO) communications [36], [38], [39]. However, the performance analyses involving Beckmann distribution are challenging since deriving the closed-form probability density function (PDF) and cumulative density function (CDF) of Beckmann distribution with unequal variances of the I/Q components is still an open problem [40]. The performance of SM-MIMO wireless communication systems has not been studied over generalized Beckmann fading channels yet, either.

IQI, as another practical key parameter that affects the system performance, has not been investigated comprehensively in the studies on SM-based MIMO communication systems. Only Rx-side IQI was introduced in [27] and [28], while only Tx-side IQI was considered in [24], assuming perfect CSI for SM wireless communication systems. However, as some of the information bits are transmitted with the active antenna indices, both Tx- and Rx-side IQI have destructive effects on the detection procedure of SM [41]. Hence, the consideration of the IQI effect only at Tx/Rx side is not enough to interpret this impairment for SM.

The lack of studies on SM-MIMO systems under the joint impact of transceiver IQI and ICSI motivates our work. This study fills in the gap by analytically evaluating the error

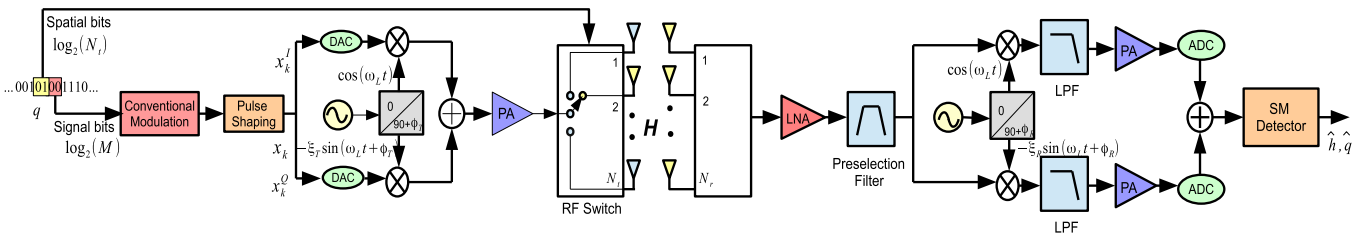

Fig. 1. The scheme of SM-MIMO wireless communication system employing a synchrodyne architecture transceiver under the effect of IQI.

performance of SM-MIMO systems while jointly taking into account those critical factors. Moreover, utilizing CRLB has provided correct estimation of CSI, and analyzing the system performance over generalized Beckmann fading channels has shed light on studies in this field.

C. Contributions

Motivated by the aforementioned factors, the contributions of this paper can be summarized as follows:

- This study investigates the error performance of SM-MIMO wireless communication systems over generalized Beckmann fading channels.
- The APEP performance of SM-MIMO wireless communication systems has been presented under the joint effect of IQI and channel impairments. The results are obtained via analytical derivations and computer simulations.
- The open problem of deriving a closed-form to the APEP over generalized Beckmann fading channels for SM-MIMO communication systems has been addressed with an upper-bound by an optimal MLD solution. Additionally, an asymptotic analysis has been conducted to get insightful findings on the impact of key parameters.
- Analytical expressions of CRLB that is specific for SM-MIMO systems have been derived for predicting and evaluating channel estimation accuracy in the presence of IQI.

Organization: The system model of SM-MIMO under the joint effect of transceiver IQI and ICSI is presented in Section II, and the optimal MLD method is given in Section III. Average and asymptotic error probability are presented in Section IV, while numerical results are provided in Section V. Finally, the study is concluded in Section VI.

Notation: Bold lower and upper case letters denote vectors and matrices, respectively. $(\cdot)^T$ and $(\cdot)^{-1}$ indicate matrix transpose and matrix inverse operations. $\mathcal{N}(\mu, \sigma^2)$ represents real Gaussian distribution with mean μ and variance σ^2. $(\cdot)^I$ and $(\cdot)^Q$ denote the I and Q components. $(\cdot)^*$ is the complex conjugate and $(\cdot)^H$ denotes the transpose conjugate, while $\mathbb{E}\{\cdot\}$ denoting the expectation. $\Re\{z\}$ stands for the real part of the complex variable z, and $\Pr\{\cdot\}$ denotes the probability of an event.

II. System and Channel Models

The scheme of the utilized SM-MIMO wireless communication system, which employs a synchrodyne architecture transceiver in the RF front-end, is given in Fig. 1. The incoming data bit stream $\boldsymbol{q}$ is divided into blocks containing $m = \log_2(N_t M)$ bits each (M is the modulation order of complex constellations and N_t is the number of Tx antennas). These blocks are further partitioned into two sub-blocks to identify the spatial and the conventional modulation bits at Tx side. Spatial bits determine a Tx antenna to switch on for transmission and RF switch block assigns the modulated signal to the activated Tx antenna. The signal passes through an $N_r \times N_t$ sized generalized Beckmann fading channel $\boldsymbol{H}$ (N_r is the number of Rx antennas), whose columns represent the complex fading gain coefficients between the i^{th} Tx antenna and the Rx antennas as vectors, i.e., $\boldsymbol{h}_i = \boldsymbol{h}_i^I + j\boldsymbol{h}_i^Q$ $(i = 1, \ldots, N_t)$.

The transmitted signal also experiences additive white Gaussian noise, $\boldsymbol{n} = \boldsymbol{n}^I + j\boldsymbol{n}^Q$, which has zero-mean independent and identical I and Q parts, i.e., $\sigma^2_{n^I} = \sigma^2_{n^Q} = \sigma^2_n/2$. The incoming signal to the Rx antenna is first amplified by a low-noise amplifier (LNA), and quadrature mixing is applied by two local oscillator (LO) signals. Afterwards, the signal on each branch is passed through a low pass filter (LPF), a power amplifier (PA) and an analog to digital converter (ADC), respectively. Then, the I and Q parts of the baseband signal are combined, and SM detector decides which symbol has been sent and which Tx antenna has been used.

A. Generalized Beckmann Fading Model

Generalized expressions of the envelope and phase distributions for two jointly correlated Gaussian random variables (RVs) are of interest in various areas of communications [42]. Thus, the real and imaginary parts of the entries of $\boldsymbol{h}_i$ are assumed to follow $\mathcal{N}(\mu_I, \sigma_I^2)$, and $\mathcal{N}(\mu_Q, \sigma_Q^2)$ distributions, respectively, based on the generalized Beckmann distribution, which considers the envelope of *correlated* Gaussian RVs with arbitrary means and non-identical variances [36].[1] The correlation coefficient between $h_{l,i}^I$ and $h_{l,i}^Q$, which represents the I/Q parts of the corresponding channel coefficients between i^{th} Tx antenna and l^{th} Rx antenna, can be calculated from:

$$\rho_h = \frac{\mathbb{E}\{(h_{l,i}^I - \mu_I)(h_{l,i}^Q - \mu_Q)\}}{\sigma_I \sigma_Q}. \tag{1}$$

Note that this extensive channel model turns into the classical Beckmann envelope fading for $\rho_h = 0$, and the PDF is

[1] A generalized Beckmann RV was defined as the square root of the quadratic sum of N correlated Gaussian RVs in [36]. In this study, the multipath fading channel model is defined by assuming $N = 2$.

written as given in (2), shown at the bottom of this page, [42]. Generalized Beckmann distribution is characterized by four parameters[2]:

$$q_B^2 \triangleq \frac{\sigma_I^2}{\sigma_Q^2}, \quad r_B^2 \triangleq \frac{\mu_I^2}{\mu_Q^2}, \quad K_B \triangleq \frac{\mu_I^2+\mu_Q^2}{\sigma_I^2+\sigma_Q^2}, \tag{3}$$

$$\Omega_B \triangleq \mu_I^2+\mu_Q^2+\sigma_I^2+\sigma_Q^2. \tag{4}$$

Here, the parameters q_B^2 and r_B^2 indicate the power imbalance between the I and Q parts of NLOS and LOS components, respectively. K_B denotes the ratio between the LOS and NLOS power, and Ω_B states the average received power. The connection between the generalized Beckmann distribution and the special cases included therein can be found in [37].

B. I/Q Imbalance Model

The I/Q mismatches mainly stem from the limited accuracy of the analog components, such as capacitors and resistors [43]. On the Tx side, this impairment can occur at the I/Q up-conversion step beside filters and digital-to-analog converters (DAC). On the Rx side, it can emerge at the down-conversion step as well as amplification and sampling stages. For simplicity, all mismatches are referred to the I/Q up- and down-conversion steps, which is typical in the literature in this context [43]–[45]. Considering both Tx and Rx IQI effects, the corresponding complex LO signals for Tx and Rx sides can be written as follows, respectively [43]:

$$\begin{aligned} z_T(t) &= \cos(\omega_L t)+j\xi_T\sin(\omega_L t+\phi_T) \\ &= G_1 e^{j\omega_L t}+G_2 e^{-j\omega_L t}, \end{aligned} \tag{5}$$

$$\begin{aligned} z_R(t) &= \cos(\omega_L t)-j\xi_R\sin(\omega_L t+\phi_R) \\ &= K_1 e^{-j\omega_L t}+K_2 e^{j\omega_L t}, \end{aligned} \tag{6}$$

where $\omega_L = 2\pi f_L$, while f_L is the LO frequency; $\{\xi_T, \phi_T\}$ and $\{\xi_R, \phi_R\}$ denote the total effective amplitude and phase imbalances of the Tx and Rx sides, respectively. IQI parameters of Tx side (G_1, G_2) and Rx side (K_1, K_2) are given in the form of:

$$G_1 = \frac{1}{2}(1+\xi_T e^{j\phi_T}), \quad G_2 = \frac{1}{2}(1-\xi_T e^{-j\phi_T}), \tag{7}$$

$$K_1 = \frac{1}{2}(1+\xi_R e^{-j\phi_R}), \quad K_2 = \frac{1}{2}(1-\xi_R e^{j\phi_R}). \tag{8}$$

Note that for perfect I/Q matching, IQI parameters reduce to $\xi_T = \xi_R = 1$ and $\phi_T = \phi_R = 0^\circ$. Therefore, in this case, it is clear that $G_1 = K_1 = 1$ and $G_2 = K_2 = 0$.

The effects of IQI can be modelled either symmetrical or asymmetrical. In the symmetrical method, each arm (I and Q) experiences half of the phase and/or amplitude errors, while the I branch is assumed to be ideal and the errors are modelled in the Q branch in the asymmetrical method [46]. It can be easily verified that these two methods are equivalent. The asymmetrical IQI structure is considered for the further analyses in this study. In this case, the baseband representation of the up-converted signal in the presence of Tx-side IQI is given as:

$$\tilde{x}_q = G_1 x_q + G_2^* x_q^*. \tag{9}$$

Here, it is assumed that M-QAM modulation scheme is utilized, and x_q is the modulated baseband Tx signal under perfect I/Q matching, where $q \in \{1, \ldots, M\}$.

Considering the frequency independent IQI model in [47], the received baseband signal at l^{th} Rx antenna is given as follows:

$$y_l = K_1(\sqrt{E}h_{l,i}\tilde{x}_q + n_l) + K_2(\sqrt{E}h_{l,i}\tilde{x}_q + n_l)^*, \tag{10}$$

where $l = \{1, \ldots, N_r\}$ and E is the transmitted signal energy. (10) can be extended to the following by considering (9):

$$\begin{aligned} y_l = {} & \sqrt{E}(K_1 G_1 h_{l,i} + K_2 G_2 h_{l,i}^*)x_q + K_1 n_l \\ & + \sqrt{E}(K_2 G_1^* h_{l,i}^* + K_1 G_2^* h_{l,i})x_q^* + K_2 n_l^*. \end{aligned} \tag{11}$$

As it is seen in (11), IQI causes a self-interference effect, $\sqrt{E}(K_2 G_1^* h_{l,i}^* + K_2 G_2^* h_{l,i})x_q^*$, beside distorting the signal. In order to clarify the destructive effect of this self-interference, assuming that symbols have unit-energy, average signal-to-interference ratio (SIR) can be calculated by using (11) as:

$$\begin{aligned} \overline{\mathrm{SIR}} &= \frac{\mathbb{E}\{|\sqrt{E}(G_1 K_1 h_{l,i} + G_2 K_2 h_{l,i}^*)|^2\}}{\mathbb{E}\{|\sqrt{E}(G_1^* K_2 h_{l,i}^* + G_2^* K_1 h_{l,i})|^2\}} \\ &= \frac{|G_1 K_1|^2 + |G_2 K_2|^2 + 2\Re\{G_1 G_2^* K_1 K_2^*\}(\sigma_I^2 - \sigma_Q^2)}{|G_2 K_1|^2 + |G_1 K_2|^2 + 2\Re\{G_1 G_2^* K_1 K_2^*\}(\sigma_I^2 - \sigma_Q^2)}. \end{aligned} \tag{12}$$

In the case of perfect I/Q matching, SIR has the ideal value of $\overline{\mathrm{SIR}} = \infty$ as seen in Fig. 2. On the contrary, even very small values of imbalance in gain, such as $\xi_T = \xi_R = 0.05$, or phase, such as $\phi_T = \phi_R = 2^\circ$, cause degradation of the SIR value. Thus, IQI needs to be considered as an important drawback of SM-MIMO wireless communication systems. On the other side, it is clear from (12) that the relationship between the variances of the I and Q components of the channel has an effect on the SIR value. Considering Fig. 2, being the parameter q_B^2, which gives the ratio between the variances of the I/Q parts of the channel, inversely proportional to the SIR value clarifies this effect.

C. Imperfect CSI Model

In practical MIMO systems, $h_{l,i}$ is not known at the Rx side and a channel estimation algorithm is used to obtain the

[2]In literature, these parameters are given as q,r,K and Ω. In order to avoid confusion with the other parameters in the paper, $(\cdot)_B$ is added here to define generalized Beckmann parameters.

$$f_{|h_{l,i}|}(h_{l,i}) = \frac{h_{l,i}}{2\pi\sigma_I\sigma_Q\sqrt{1-\rho_h^2}}\int_0^{2\pi}\exp\left\{-\frac{1}{2(1-\rho_h^2)}\times\left[\left(\frac{h_{l,i}^I-\mu_I}{\sigma_I}\right)^2-\left(\frac{h_{l,i}^Q-\mu_Q}{\sigma_Q}\right)^2-\frac{2\rho_h(h_{l,i}^I-\mu_I)(h_{l,i}^Q-\mu_Q)}{\sigma_I\sigma_Q}\right]\right\}d\theta \tag{2}$$

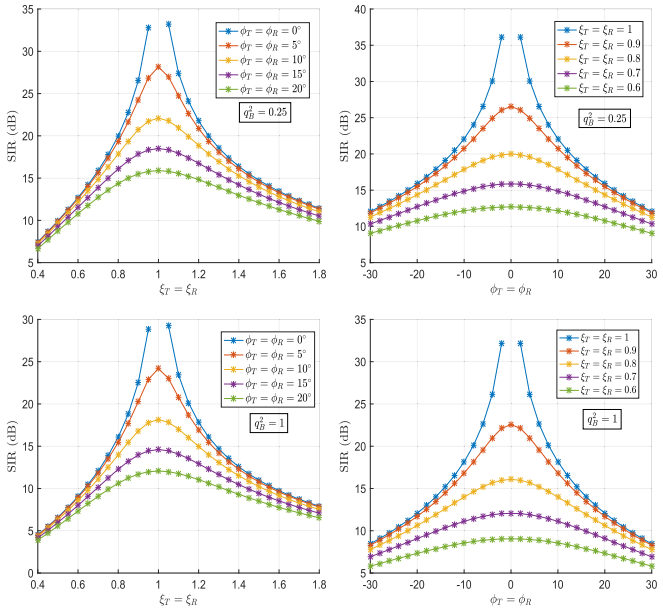

Fig. 2. SIR values given for IQI affected SM-MIMO system with fixed values of phase imbalance (first column) and fixed values of amplitude imbalance (second column).

estimated channel matrix $\tilde{\boldsymbol{H}}$ [48]. It is assumed that the generalized Beckmann channel components, $h_{l,i}$, and the estimated versions of them, $\tilde{h}_{l,i}$, are jointly ergodic and stationary.

Assuming that the actual channel and the estimation error are orthogonal as well, a common estimation rule is considered, and given as [31], [49], [50]:

$$h_{l,i} = \tilde{h}_{l,i} - e_l, \tag{13}$$

where e_l denotes the channel estimation error, which has correlated I and Q parts modeled as $\mathcal{N}\left(0, \sigma_{e^I}^2\right)$, and $\mathcal{N}\left(0, \sigma_{e^Q}^2\right)$ respectively. Here, it is worth noting that $\sigma_e^2 = \mathbb{E}[|e_l|^2] = \sigma_{e^I}^2 + \sigma_{e^Q}^2$ indicates the quality of the estimation and can be chosen depending on the channel dynamics and estimation methods [48], [51]. In this study, CRB method, which is discussed in Section-D, has been utilized for estimation of $\sigma_{e^I}^2$ and $\sigma_{e^Q}^2$.

Considering (13), it can be seen that the estimated channel coefficients have correlated I and Q parts with:

$$\rho_{\tilde{h}} = \frac{\mathbb{E}\{(h_{l,i}^I - \mu_I)(h_{l,i}^Q - \mu_Q)\} + \mathbb{E}\{e_l^I e_l^Q\}}{\sqrt{(\sigma_I^2 + \sigma_{e^I}^2)(\sigma_Q^2 + \sigma_{e^Q}^2)}}. \tag{14}$$

(10) can be rewritten by using (13) as follows:

$$\begin{aligned}\boldsymbol{y} &= \sqrt{E}[K_1(\tilde{\boldsymbol{h}}_i - \boldsymbol{e})\tilde{x}_q + K_2(\tilde{\boldsymbol{h}}_i - \boldsymbol{e})^*\tilde{x}_q^*] + K_1\boldsymbol{n} + K_2\boldsymbol{n}^* \\ &= \sqrt{E}\tilde{\boldsymbol{\chi}}_p + \tilde{\boldsymbol{n}}.\end{aligned} \tag{15}$$

Here $\tilde{\boldsymbol{\chi}}_p = K_1\tilde{\boldsymbol{h}}_i\tilde{x}_q + K_2\tilde{\boldsymbol{h}}_i^*\tilde{x}_q^*$, $p \in \{1, \ldots, m\}$, and the noise part of $\boldsymbol{y}$ equals to $\tilde{\boldsymbol{n}} = -\sqrt{E}K_1\boldsymbol{e}\tilde{x}_q + \sqrt{E}K_2\boldsymbol{e}^*\tilde{x}_q^* + K_1\boldsymbol{n} + K_2\boldsymbol{n}^*$.

At this point, note that if a complex Gaussian RV is not circularly-symmetric, it is referred to as improper [52]. Improper characteristics of a complex Gaussian RV is based on the existence of at least one of these two conditions: i) real and imaginary parts are correlated, ii) real and imaginary parts do not have the same variance (non-identical). Hence, it is seen that $\tilde{\boldsymbol{n}}$ in (15) has correlated I/Q components, since $\mathrm{cov}(\tilde{n}_l^I, \tilde{n}_l^Q) \neq 0$, and the correlation coefficient can be calculated form [28]:

$$\rho_{\tilde{n}} = \frac{\mathrm{cov}(\tilde{n}_l^I, \tilde{n}_l^Q)}{\sigma_{\tilde{n}_l^I}\sigma_{\tilde{n}_l^Q}}. \tag{16}$$

Although just having correlated components is enough to remark that $\tilde{\boldsymbol{n}}$ is an improper Gaussian noise, the second condition, being non-identical, is valid for it as well, since the variance values of I and Q parts of $\tilde{\boldsymbol{n}}$ are calculated as follows:

$$\begin{aligned}\sigma_{\tilde{n}_l^I}^2 &= E[|\tilde{x}_q^I|^2\sigma_{e^I}^2 + |\tilde{x}_q^Q|^2\sigma_{e^Q}^2 - 2\mathbb{E}\{e_l^I e_l^Q\}\tilde{x}_q^I\tilde{x}_q^Q] + \frac{\sigma_n^2}{2}, \\ \sigma_{\tilde{n}_l^Q}^2 &= E[\sigma_{e^I}^2|K_c\tilde{x}_q^I + K_d\tilde{x}_q^Q|^2 + \sigma_{e^Q}^2|K_d\tilde{x}_q^I - K_c\tilde{x}_q^Q|^2 \\ &\quad + 2\mathbb{E}\{e_l^I e_l^Q\}(K_c\tilde{x}_q^I + K_d\tilde{x}_q^Q)(K_d\tilde{x}_q^I - K_c\tilde{x}_q^Q)] + \frac{\xi_R^2\sigma_n^2}{2}.\end{aligned} \tag{17}$$

where $K_c = K_1^Q + K_2^Q$ and $K_d = K_1^I - K_2^I$. Therefore, the variances of I and Q parts of $\tilde{n}$ are non-identical. Here, it is worth nothing that the traditional MLD can not provide an optimum solution since it has been derived by assuming proper Gaussain noise characteristics.

D. Cramer-Rao Lower Bound (CRLB) of SM-MIMO With IQI and ICSI

The CRLB is a performance criterion that gives a lower bound to the variance of estimation error in a set of unbiased estimates [30]. In this section, pilot symbols insertion is introduced to perform channel estimation for coherent detection and an exact CRLB expression, which is used not only to evaluate but also to predict the estimator performance, is derived.

The exact Fisher information matrix (FIM) of the channel estimation that measures the sensitivity of the channel model to changes of $\boldsymbol{h}_i$ [53], is given as [30]:

$$\begin{aligned}I_{(\boldsymbol{h}_i)}(\boldsymbol{h}_i) &= \mathbb{E}\left\{\left[\frac{\partial \ln P_{\boldsymbol{y}}(\tilde{\boldsymbol{y}}; \boldsymbol{h}_i)}{\partial \boldsymbol{h}_i^*}\right]\left[\frac{\partial \ln P_{\boldsymbol{y}}(\tilde{\boldsymbol{y}}; \boldsymbol{h}_i)}{\partial \boldsymbol{h}_i^*}\right]^H\right\} \\ &= \begin{bmatrix} I_{(\boldsymbol{h}_i^I)} & I_{(\boldsymbol{h}_i^I, \boldsymbol{h}_i^Q)} \\ I_{(\boldsymbol{h}_i^Q, \boldsymbol{h}_i^I)} & I_{(\boldsymbol{h}_i^Q)} \end{bmatrix},\end{aligned} \tag{18}$$

where $P_{\boldsymbol{y}}(\tilde{\boldsymbol{y}}; \boldsymbol{h}_i)$ is the likelihood function of the unknown channel $\boldsymbol{h}_i$, which is also equal to the joint PDF of N_p obsevations based on an observation vector $\tilde{\boldsymbol{y}} = [y(1)\ y(2)\ \ldots\ y(N_p)]^T$, and $I_{(\boldsymbol{h}_i^I, \boldsymbol{h}_i^Q)} = I_{(\boldsymbol{h}_i^Q, \boldsymbol{h}_i^I)}$. In this expression, $I_{(\boldsymbol{h}_i^I)}$, $I_{(\boldsymbol{h}_i^Q)}$ and $I_{(\boldsymbol{h}_i^I, \boldsymbol{h}_i^Q)}$ values are calculated as follows for the proposed SM model:

$$\begin{aligned}I_{(\boldsymbol{h}_i^I)} = \frac{N_p E}{1 - \rho_\eta^2}\Bigg[&\frac{(\tilde{x}_q^I)^2}{\sigma_{\eta^I}^2} + \frac{(\tilde{x}_q^I K_c + \tilde{x}_q^Q K_d)^2}{\sigma_{\eta^Q}^2} \\ &- \frac{2\rho_\eta\tilde{x}_q^I(\tilde{x}_q^I K_c + \tilde{x}_q^Q K_d)}{\sigma_{\eta^I}\sigma_{\eta^Q}}\Bigg],\end{aligned} \tag{19}$$

$$I_{(\boldsymbol{h}_i^Q)} = \frac{N_p E}{1-\rho_\eta^2}\Bigg[\frac{(\tilde{x}_q^Q)^2}{\sigma_{\eta^I}^2} + \frac{(\tilde{x}_q^I K_d - \tilde{x}_q^Q K_c)^2}{\sigma_{\eta^Q}^2} - \frac{2\rho_\eta \tilde{x}_q^Q(\tilde{x}_q^I K_d - \tilde{x}_q^Q K_c)}{\sigma_{\eta^I}\sigma_{\eta^Q}}\Bigg], \tag{20}$$

$$I_{(\boldsymbol{h}_i^I,\boldsymbol{h}_i^Q)} = \frac{N_p E}{1-\rho_\eta^2}\Bigg[\frac{-\tilde{x}_q^I\tilde{x}_q^Q}{\sigma_{\eta^I}^2} + \frac{(\tilde{x}_q^I K_d - \tilde{x}_q^Q K_c)(\tilde{x}_q^I K_c + \tilde{x}_q^Q K_d)}{\sigma_{\eta^Q}^2} + \frac{\rho_\eta(\tilde{x}_q^Q(\tilde{x}_q^I K_c + \tilde{x}_q^Q K_d) + \tilde{x}_q^I(\tilde{x}_q^I K_d - \tilde{x}_q^Q K_c))}{\sigma_{\eta^I}\sigma_{\eta^Q}}\Bigg], \tag{21}$$

where N_P is the number of pilot symbols, and $\rho_\eta = -\sin\phi_R$. Details on the mathematical background to obtain these values are given in Appendix-A.

CRLB matrix can be obtained by utilizing (18), and it provides a lower bound for the covariance matrix of the estimation error, which includes the variance values of the real and imaginary parts, as follows:

$$\mathrm{CRLB}_i = [I_{(\boldsymbol{h}_i)}(\boldsymbol{h}_i)]_i^{-1} = \begin{bmatrix} \sigma_{e^I}^2 & \mathbb{E}\{e^I e^Q\} \\ \mathbb{E}\{e^I e^Q\} & \sigma_{e^Q}^2 \end{bmatrix}. \tag{22}$$

III. Optimal Maximum Likelihood Detector Design

In this section, an optimal MLD design is introduced for the presented SM-MIMO wireless communication system operating under the effects of IQI and ICSI. The destructive effects of these impairments are modeled as improper Gaussian as mentioned in Section II-C, and this allows us to analyze the asymmetric characteristics of the IQI accurately [54]. Since it is proven that utilizing the improperness of the Gaussian noise using MLD method leads to a decrease in the error probability [55], the optimal MLD scheme is designed by considering this phenomenon. Additionally, it is assumed that the IQI parameters are known at the Rx-side during the formulation.

The joint multi-variate PDF of the real part and the imaginary part of the received signal, $\boldsymbol{y}$, which is under the effect of both Tx- and Rx-side IQI as well as ICSI, can be expressed by using (15) as follows [28]:

$$f_{\boldsymbol{y}^I,\boldsymbol{y}^Q}(\boldsymbol{y}^I,\boldsymbol{y}^Q|\tilde{\boldsymbol{\chi}}_p) = \left(\frac{1}{2\pi\sigma_{\tilde{n}_l^I}\sigma_{\tilde{n}_l^Q}\sqrt{1-\rho_{\tilde{n}}^2}}\right)^{N_r} \times \exp\left(\frac{-1}{2(1-\rho_{\tilde{n}}^2)}\left[\frac{\|\boldsymbol{y}^I-\sqrt{E}\tilde{\boldsymbol{\chi}}_p^I\|^2}{\sigma_{\tilde{n}_l^I}^2} + \frac{\|\boldsymbol{y}^Q-\sqrt{E}\tilde{\boldsymbol{\chi}}_p^Q\|^2}{\sigma_{\tilde{n}_l^Q}^2} - \frac{2\rho_{\tilde{n}}(\boldsymbol{y}^I-\sqrt{E}\tilde{\boldsymbol{\chi}}_p^I)^T(\boldsymbol{y}^Q-\sqrt{E}\tilde{\boldsymbol{\chi}}_p^Q)}{\sigma_{\tilde{n}_l^I}\sigma_{\tilde{n}_l^Q}}\right]\right). \tag{23}$$

Hence, the optimal MLD decision rule, assuming equiprobable symbols, can be defined by:

$$\hat{p} = \arg\max_p\{f_{\boldsymbol{y}^I,\boldsymbol{y}^Q}(\boldsymbol{y}^I,\boldsymbol{y}^Q|\tilde{\boldsymbol{\chi}}_p)\} = \arg\min_p\left\{\frac{\|\boldsymbol{y}^I-\sqrt{E}\tilde{\boldsymbol{\chi}}_p^I\|^2}{\sigma_{\tilde{n}_l^I}^2} + \frac{\|\boldsymbol{y}^Q-\sqrt{E}\tilde{\boldsymbol{\chi}}_p^Q\|^2}{\sigma_{\tilde{n}_l^Q}^2} - \frac{2\rho_{\tilde{n}}(\boldsymbol{y}^I-\sqrt{E}\tilde{\boldsymbol{\chi}}_p^I)^T(\boldsymbol{y}^Q-\sqrt{E}\tilde{\boldsymbol{\chi}}_p^Q)}{\sigma_{\tilde{n}_l^I}\sigma_{\tilde{n}_l^Q}}\right\}, \tag{24}$$

which jointly counts the error in Tx antenna indices and symbols.

IV. Error Performance Analysis

A. Average Pairwise Error Probability (APEP)

Considering the optimal MLD rule given in (24), the conditional pairwise error probability (PEP) can be calculated from (25) under the assumption that $\tilde{\boldsymbol{\chi}}_p$ has been transmitted; however, $\hat{\boldsymbol{\chi}}_p$ is detected erroneously at the Rx side:

$$\Pr\left(\tilde{\boldsymbol{\chi}}_p \to \hat{\boldsymbol{\chi}}_p|\tilde{\boldsymbol{H}}\right) = \Pr\left(\frac{\|\boldsymbol{y}^I-\sqrt{E}\tilde{\boldsymbol{\chi}}_p^I\|^2}{\sigma_{\tilde{n}_l^I}^2} + \frac{\|\boldsymbol{y}^Q-\sqrt{E}\tilde{\boldsymbol{\chi}}_p^Q\|^2}{\sigma_{\tilde{n}_l^Q}^2} - \frac{2\rho_{\tilde{n}}(\boldsymbol{y}^I-\sqrt{E}\tilde{\boldsymbol{\chi}}_p^I)^T(\boldsymbol{y}^Q-\sqrt{E}\tilde{\boldsymbol{\chi}}_p^Q)}{\sigma_{\tilde{n}_l^I}\sigma_{\tilde{n}_l^Q}} > \frac{\|\boldsymbol{y}^I-\sqrt{E}\hat{\boldsymbol{\chi}}_p^I\|^2}{\sigma_{\tilde{n}_l^I}^2} + \frac{\|\boldsymbol{y}^Q-\sqrt{E}\hat{\boldsymbol{\chi}}_p^Q\|^2}{\sigma_{\tilde{n}_l^Q}^2} - \frac{2\rho_{\tilde{n}}(\boldsymbol{y}^I-\sqrt{E}\hat{\boldsymbol{\chi}}_p^I)^T(\boldsymbol{y}^Q-\sqrt{E}\hat{\boldsymbol{\chi}}_p^Q)}{\sigma_{\tilde{n}_l^I}\sigma_{\tilde{n}_l^Q}}\right). \tag{25}$$

Here, $\hat{\boldsymbol{\chi}}_p = K_1\hat{\tilde{\boldsymbol{h}}}_i\hat{\tilde{x}}_q + K_2\hat{\tilde{\boldsymbol{h}}}_i^*\hat{\tilde{x}}_q^*$ and $\hat{\tilde{\boldsymbol{h}}}_i$ is the complex channel coefficient related to detected Tx antenna that transmits the detected signal $\hat{\tilde{x}}_q$. After some algebraic simplifications, it is obtained that:

$$\begin{aligned}\mathrm{PEP} &= \Pr\Bigg(\frac{2\rho_{\tilde{n}}\sqrt{E}\{(\tilde{\boldsymbol{\chi}}_p^I-\hat{\boldsymbol{\chi}}_p^I)^T\tilde{\boldsymbol{n}}_l^Q + (\tilde{\boldsymbol{\chi}}_p^Q-\hat{\boldsymbol{\chi}}_p^Q)^T\tilde{\boldsymbol{n}}_l^I\}}{\sigma_{\tilde{n}_l^I}\sigma_{\tilde{n}_l^Q}} - \frac{2\sqrt{E}(\tilde{\boldsymbol{\chi}}_p^I-\hat{\boldsymbol{\chi}}_p^I)^T\tilde{\boldsymbol{n}}_l^I}{\sigma_{\tilde{n}_l^I}^2} - \frac{2\sqrt{E}(\tilde{\boldsymbol{\chi}}_p^Q-\hat{\boldsymbol{\chi}}_p^Q)^T\tilde{\boldsymbol{n}}_l^Q}{\sigma_{\tilde{n}_l^Q}^2} \\ &\quad - \frac{E\|\tilde{\boldsymbol{\chi}}_p^I-\hat{\boldsymbol{\chi}}_p^I\|^2}{\sigma_{\tilde{n}_l^I}^2} - \frac{E\|\tilde{\boldsymbol{\chi}}_p^Q-\hat{\boldsymbol{\chi}}_p^Q\|^2}{\sigma_{\tilde{n}_l^Q}^2} + \frac{2\rho_{\tilde{n}}E\left(\tilde{\boldsymbol{\chi}}_p^I-\hat{\boldsymbol{\chi}}_p^I\right)^T\left(\tilde{\boldsymbol{\chi}}_p^Q-\hat{\boldsymbol{\chi}}_p^Q\right)}{\sigma_{\tilde{n}_l^I}\sigma_{\tilde{n}_l^Q}} > 0\Bigg) \\ &= \Pr(\mathcal{G}>0),\end{aligned} \tag{26}$$

where $\mathcal{G}$, conditioned on $\tilde{\boldsymbol{\chi}}_p$, is a Gaussian RV. Now, PEP can be defined by using the mean, $\mu_\mathcal{G}$, and variance, $\sigma_\mathcal{G}^2$, values of the $\mathcal{G}$, and the well-known Q-function[3] as:

$$\mathrm{PEP} = Q\left(\frac{\mathbb{E}\{\mathcal{G}\}}{\sqrt{\mathrm{var}(\mathcal{G})}}\right) = Q\left(\frac{\mu_\mathcal{G}}{\sigma_\mathcal{G}}\right). \tag{27}$$

Here, $\mu_\mathcal{G}$ and $\sigma_\mathcal{G}^2$ are obtained respectively as follows:

$$\mu_\mathcal{G} = \left(\frac{E\|\tilde{\boldsymbol{\chi}}_p^I-\hat{\boldsymbol{\chi}}_p^I\|^2}{\sigma_{\tilde{n}_l^I}^2} + \frac{E\|\tilde{\boldsymbol{\chi}}_p^Q-\hat{\boldsymbol{\chi}}_p^Q\|^2}{\sigma_{\tilde{n}_l^Q}^2} - \frac{2\rho_{\tilde{n}}E\left(\tilde{\boldsymbol{\chi}}_p^I-\hat{\boldsymbol{\chi}}_p^I\right)^T\left(\tilde{\boldsymbol{\chi}}_p^Q-\hat{\boldsymbol{\chi}}_p^Q\right)}{\sigma_{\tilde{n}_l^I}\sigma_{\tilde{n}_l^Q}}\right), \tag{28}$$

$$\sigma_\mathcal{G}^2 = 4E(1-\rho_{\tilde{n}}^2)\times\left(\frac{\|\tilde{\boldsymbol{\chi}}_p^I-\hat{\boldsymbol{\chi}}_p^I\|^2}{\sigma_{\tilde{n}_l^I}^2} + \frac{\|\tilde{\boldsymbol{\chi}}_p^Q-\hat{\boldsymbol{\chi}}_p^Q\|^2}{\sigma_{\tilde{n}_l^Q}^2} - \frac{2\rho_{\tilde{n}}\left(\tilde{\boldsymbol{\chi}}_p^I-\hat{\boldsymbol{\chi}}_p^I\right)^T\left(\tilde{\boldsymbol{\chi}}_p^Q-\hat{\boldsymbol{\chi}}_p^Q\right)}{\sigma_{\tilde{n}_l^I}\sigma_{\tilde{n}_l^Q}}\right). \tag{29}$$

[3] $Q(x)$ is defined as $Q(x) = \frac{1}{\sqrt{2\pi}}\int_x^\infty e^{-t^2/2}dt$.

Substituting (28) and (29) in (27), the conditional PEP can be given as in (30), shown at the bottom of this page. Although the average PEP (APEP) can be defined by using the expected value of the PEP expression of (30) as given in (31), it is not relatively easy to find $f_\gamma(\gamma)$, which is the PDF of $\boldsymbol{\gamma}$, in the following expression:

$$\begin{aligned}\text{APEP} &= \mathbb{E}\left\{Q\left(\sqrt{\frac{E\boldsymbol{\gamma}}{4(1-\rho_{\tilde{n}}^2)}}\right)\right\}\\ &= \int_{-\infty}^{\infty} Q\left(\sqrt{\frac{E\boldsymbol{\gamma}}{4(1-\rho_{\tilde{n}}^2)}}\right) f_\gamma(\gamma)d\gamma. \end{aligned} \tag{31}$$

Therefore, the moment generating function[4] (MGF), which provides an alternative solution instead of using the Q-function, is utilized to find APEP in this study. In order to define the MGF of $\boldsymbol{\gamma}$, (30) can be simplified as:

$$\text{PEP} = Q\left(\sqrt{\frac{E}{4(1-\rho_{\tilde{n}}^2)}\left(\frac{\|\boldsymbol{\zeta}_1\|^2}{\sigma^2_{\tilde{n}_l^I}}+\frac{\|\boldsymbol{\zeta}_2\|^2}{\sigma^2_{\tilde{n}_l^Q}}-\frac{2\rho_{\tilde{n}}\boldsymbol{\zeta}_1^T\boldsymbol{\zeta}_2}{\sigma_{\tilde{n}_l^I}\sigma_{\tilde{n}_l^Q}}\right)}\right), \tag{32}$$

where $\boldsymbol{\gamma} = \frac{\|\boldsymbol{\zeta}_1\|^2}{\sigma^2_{\tilde{n}_l^I}} + \frac{\|\boldsymbol{\zeta}_2\|^2}{\sigma^2_{\tilde{n}_l^Q}} - \frac{2\rho_{\tilde{n}}\boldsymbol{\zeta}_1^T\boldsymbol{\zeta}_2}{\sigma_{\tilde{n}_l^I}\sigma_{\tilde{n}_l^Q}}$, $\boldsymbol{\zeta}_1 = (\tilde{\boldsymbol{\chi}}_p^I - \hat{\boldsymbol{\chi}}_p^I)$ and $\boldsymbol{\zeta}_2 = (\tilde{\boldsymbol{\chi}}_p^Q - \hat{\boldsymbol{\chi}}_p^Q)$, while $\boldsymbol{\zeta}_1$ and $\boldsymbol{\zeta}_2$ follow $\mathcal{N}(\mu_1, \upsilon_1)$ and $\mathcal{N}(\mu_2, \upsilon_2)$, respectively. Here, it should be noted that if the value of error variance is adjusted as proportional to $1/E$ in (17), the effect of error variance on the PEP in (32) would be cancelled. In other words, the denominator in (32) decreases in this case, since the transmitted energy increases, thereby decreasing the error probability.

The mean values of ζ_1 and ζ_2 are calculated as:

$$\begin{aligned}\mu_1 &= \mu_I(\tilde{x}_q^I - \hat{\tilde{x}}_q^I) + \mu_Q(\hat{\tilde{x}}_q^Q - \tilde{x}_q^Q),\\ \mu_2 &= \mu_I(K_c\tilde{x}_q^I + K_d\tilde{x}_q^Q - K_c\hat{\tilde{x}}_q^I - K_d\hat{\tilde{x}}_q^Q)\\ &\quad +\mu_Q(K_d\tilde{x}_q^I - K_c\tilde{x}_q^Q - K_d\hat{\tilde{x}}_q^I + K_c\hat{\tilde{x}}_q^Q). \end{aligned} \tag{33}$$

Representing $\hat{i}$ as the index of the detected Tx antenna, which is used to convey the modulated signal, the variance values υ_1 and υ_2 are obtained depending on two cases:

Case 1: $i = \hat{i}$

$$\begin{aligned}\upsilon_1 &= (\sigma_I^2 + \sigma_{e^I}^2)|\tilde{x}_q^I - \hat{\tilde{x}}_q^I|^2 + (\sigma_Q^2 + \sigma_{e^Q}^2)|\hat{\tilde{x}}_q^Q - \tilde{x}_q^Q|^2\\ &\quad +2\mathbb{E}\{\tilde{h}_{l,i}^I\tilde{h}_{l,i}^Q\}(\tilde{x}_q^I - \hat{\tilde{x}}_q^I)(\hat{\tilde{x}}_q^Q - \tilde{x}_q^Q)\end{aligned}$$

$$\begin{aligned}\upsilon_2 &= (\sigma_I^2 + \sigma_{e^I}^2)|K_c(\tilde{x}_q^I - \hat{\tilde{x}}_q^I) + K_d(\tilde{x}_q^Q - \hat{\tilde{x}}_q^Q)|^2\\ &\quad +(\sigma_Q^2 + \sigma_{e^Q}^2)|K_d(\tilde{x}_q^I - \hat{\tilde{x}}_q^I) + K_c(\hat{\tilde{x}}_q^Q - \tilde{x}_q^Q)|^2\\ &\quad +2\mathbb{E}\{\tilde{h}_{l,i}^I\tilde{h}_{l,i}^Q\} \times [K_c(\tilde{x}_q^I - \hat{\tilde{x}}_q^I) + K_d(\tilde{x}_q^Q - \hat{\tilde{x}}_q^Q)]\\ &\quad \times[K_d(\tilde{x}_q^I - \hat{\tilde{x}}_q^I) + K_c(\hat{\tilde{x}}_q^Q - \tilde{x}_q^Q)]\end{aligned} \tag{34}$$

Case 2: $i \neq \hat{i}$

$$\begin{aligned}\upsilon_1 &= (\sigma_I^2 + \sigma_{e^I}^2)(|\tilde{x}_q^I|^2 + |\hat{\tilde{x}}_q^I|^2) + (\sigma_Q^2 + \sigma_{e^Q}^2)(|\hat{\tilde{x}}_q^Q|^2 + |\tilde{x}_q^Q|^2)\\ &\quad -2\mathbb{E}\{\tilde{h}_{l,i}^I\tilde{h}_{l,i}^Q\}(\tilde{x}_q^I\tilde{x}_q^Q + \hat{\tilde{x}}_q^I\hat{\tilde{x}}_q^Q)\\ \upsilon_2 &= (\sigma_I^2 + \sigma_{e^I}^2)(|K_c\tilde{x}_q^I + K_d\tilde{x}_q^Q|^2 + |K_c\hat{\tilde{x}}_q^I + K_d\hat{\tilde{x}}_q^Q|^2)\\ &\quad +(\sigma_Q^2 + \sigma_{e^Q}^2)(|K_d\tilde{x}_q^I - K_c\tilde{x}_q^Q|^2 + |K_d\hat{\tilde{x}}_q^I - K_c\hat{\tilde{x}}_q^Q|^2)\\ &\quad +2\mathbb{E}\{\tilde{h}_{l,i}^I\tilde{h}_{l,i}^Q\} \times [(K_c\tilde{x}_q^I + K_d\tilde{x}_q^Q)(K_d\tilde{x}_q^I - K_c\tilde{x}_q^Q)\\ &\quad +(K_c\hat{\tilde{x}}_q^I + K_d\hat{\tilde{x}}_q^Q)(K_d\hat{\tilde{x}}_q^I - K_c\hat{\tilde{x}}_q^Q)].\end{aligned} \tag{35}$$

Noting that $\boldsymbol{\gamma}$ is a linear combination of two correlated noncentral chi-squared RVs with one degree of freedom, $\boldsymbol{\gamma}$ can be written in a quadratic form of Gaussian RVs, which is given in more detail in Appendix B. Thus, the MGF of $\boldsymbol{\gamma}$ is given as follows under the assumption of independent channels [56]:

$$M_{\boldsymbol{\gamma}}(t) = \left(\frac{\exp\left(\frac{b_1^2\lambda_1 t}{1-2\lambda_1 t}\right)}{\sqrt{1-2\lambda_1 t}} \times \frac{\exp\left(\frac{b_2^2\lambda_2 t}{1-2\lambda_2 t}\right)}{\sqrt{1-2\lambda_2 t}}\right)^{N_r}, \tag{36}$$

where b_1 and b_2 are the mean values and λ_1 and λ_2 are the eigenvalues all calculated based on the covariance matrix of $\boldsymbol{\zeta}_1$ and $\boldsymbol{\zeta}_2$, and given in Appendix B.

In light of this information, the APEP can be calculated analytically by using (36) from:

$$\text{APEP} = \Pr(\tilde{\boldsymbol{\chi}}_p \to \hat{\boldsymbol{\chi}}_p) = \frac{1}{\pi}\int_0^{\frac{\pi}{2}} M_{\boldsymbol{\gamma}}\left(\frac{-E}{8(1-\rho_{\tilde{n}}^2)\sin^2\theta}\right)d\theta. \tag{37}$$

This integral can be easily solved via numerical methods. Furthermore, considering the maximum value of $\sin^2\theta = 1$ [57, p. 230], this integration can be upper-bounded as:

$$\text{APEP} \leq \frac{1}{2}M_{\boldsymbol{\gamma}}\left(\frac{-E}{8(1-\rho_{\tilde{n}}^2)}\right). \tag{38}$$

Consequently, a closed-form upper-bound, as given in (39), shown at the bottom of this page, is obtained by using (36) and (38).

[4]Assuming that $\overline{\gamma}$ equals to the SNR of any γ, MGF of γ, stated by M, can be utilized as an alternative representation of Q-function as follows: $\int_{-\infty}^{\infty} Q(\sqrt{\overline{\gamma}\gamma})f_\gamma(\gamma)d\gamma = \frac{1}{\pi}\int_0^{\frac{\pi}{2}} M(-\frac{\overline{\gamma}}{2\sin^2\theta})d\theta$.

$$\text{PEP} = Q\left(\sqrt{\frac{E}{4(1-\rho_{\tilde{n}}^2)}\left(\frac{\|\tilde{\boldsymbol{\chi}}_p^I - \hat{\boldsymbol{\chi}}_p^I\|^2}{\sigma^2_{\tilde{n}_l^I}} + \frac{\|\tilde{\boldsymbol{\chi}}_p^Q - \hat{\boldsymbol{\chi}}_p^Q\|^2}{\sigma^2_{\tilde{n}_l^Q}} - \frac{2\rho_{\tilde{n}}\left(\tilde{\boldsymbol{\chi}}_p^I - \hat{\boldsymbol{\chi}}_p^I\right)^T(\tilde{\boldsymbol{\chi}}_p^Q - \hat{\boldsymbol{\chi}}_p^Q)}{\sigma_{\tilde{n}_l^I}\sigma_{\tilde{n}_l^Q}}\right)}\right) = Q\left(\sqrt{\frac{E\boldsymbol{\gamma}}{4(1-\rho_{\tilde{n}}^2)}}\right) \tag{30}$$

$$\text{APEP} \leq \frac{1}{2}\left(\frac{8(1-\rho_{\tilde{n}}^2)\exp\left(-\frac{b_1^2\lambda_1 E}{8(1-\rho_{\tilde{n}}^2)+2\lambda_1 E} - \frac{b_2^2\lambda_2 E}{8(1-\rho_{\tilde{n}}^2)+2\lambda_2 E}\right)}{\sqrt{[8(1-\rho_{\tilde{n}}^2)+2\lambda_1 E][8(1-\rho_{\tilde{n}}^2)+2\lambda_2 E]}}\right) \tag{39}$$

B. Asymptotic Analysis

Assuming $E \gg 1$, an asymptotic APEP is provided by utilizing (36) and (37) as follows:

$$\mathrm{APEP}_{\mathrm{asy}} = \frac{1}{\pi}\left(\frac{\exp(-\frac{b_1^2+b_2^2}{2})}{[E/4(1-\rho_{\tilde{n}}^2)]\sqrt{\lambda_1\lambda_2}}\right)^{N_r}\int_0^{\frac{\pi}{2}}(\sin\theta)^{2N_r}d\theta. \tag{40}$$

This expression proves that APEP depends on the number of Rx antennas, the mean values based on the generalized Beckmann fading channel, the energy of the transmitted signal, the correlation between the I/Q parts of the improper Gaussian noise and the eigenvalues that calculated based on the covariance matrix of $\boldsymbol{\zeta}_1$ and $\boldsymbol{\zeta}_2$.

Considering that $B(N_r+\frac{1}{2},\frac{1}{2}) = 2\int_0^{\frac{\pi}{2}}(\sin\theta)^{2N_r}d\theta$ [58, Eq. 8.308(2)] and $B(N_r+\frac{1}{2},\frac{1}{2}) = \frac{\Gamma(N_r+\frac{1}{2})\Gamma(\frac{1}{2})}{\Gamma(N_r+1)}$ [58, Eq. 8.384(1)], one has $\int_0^{\frac{\pi}{2}}(\sin\theta)^{2N_r}d\theta = \frac{\sqrt{\pi}\,\Gamma(N_r+\frac{1}{2})}{2\Gamma(N_r+1)}$, where $B(\cdot,\cdot)$ and $\Gamma(\cdot)$ are the Beta function and the Gamma function, respectively. Considering also that $\Gamma(N_r+1)=N_r!$ [59, Eq. 1.1.7] and $\Gamma(N_r+\frac{1}{2}) = \frac{\sqrt{\pi}(2N_r-1)!!}{2^{N_r}}$ [60, p.509], (40) can be rewritten as:

$$\mathrm{APEP}_{\mathrm{asy}} = \Xi\left(\frac{E}{4(1-\rho_{\tilde{n}})}\right)^{-N_r}, \tag{41}$$

where $\Xi = \frac{(2N_r-1)!!}{2^{N_r+1}N_r!}\left(\frac{\exp(-\frac{b_1^2+b_2^2}{2})}{\sqrt{\lambda_1\lambda_2}}\right)^{N_r}$ can be calculated as a constant value, and $\frac{E}{4(1-\rho_{\tilde{n}})}$ is equal to signal-to-noise ratio (SNR) that can be seen in (30).

Now, the diversity gain can be calculated from:

$$g = -\lim_{\mathrm{SNR}\to\infty}\frac{\log(\mathrm{APEP}_{\mathrm{asy}})}{\log(\mathrm{SNR})}. \tag{42}$$

Substituting (41) in (42) proves that the diversity gain is equal to the number of Rx antennas, N_r, while the error variance decreases with the energy, as such in the case of perfect I/Q match.

C. Average Bit Error Rate

After the evaluation of the APEP, the ABER of the proposed scheme can be given under the assumption of equiprobable symbols by using well-known tight union bound method as follows [28]:

$$\mathrm{ABER} \le \frac{1}{2^m}\sum_{n=1}^{2^m}\sum_{\substack{k=1\\ n\neq k}}^{2^m}\frac{\Pr(\tilde{\boldsymbol{\chi}}_p \to \hat{\boldsymbol{\chi}}_p)\, e_{n,k}}{m}, \tag{43}$$

where $e_{n,k}$ is the number of bit errors relevant to the corresponding pairwise error event.

V. Numerical Results

In this section, the joint effect of IQI and ICSI on the performance of the SM-MIMO wireless communication system is evaluated over generalized Beckmann fading channels by using the proposed optimal MLD design through computer simulations and analytical derivations. It is assumed that at least 5×10^5 symbols have been transmitted for each SNR value, which is defined as E/σ_n^2, between $0-30$ dB. 4-QAM modulation scheme is utilized on SM wireless communication system with one Rx antenna because of the simplicity, unless otherwise stated; however, all results can be generalized for any number of Rx antennas and higher order modulation schemes.

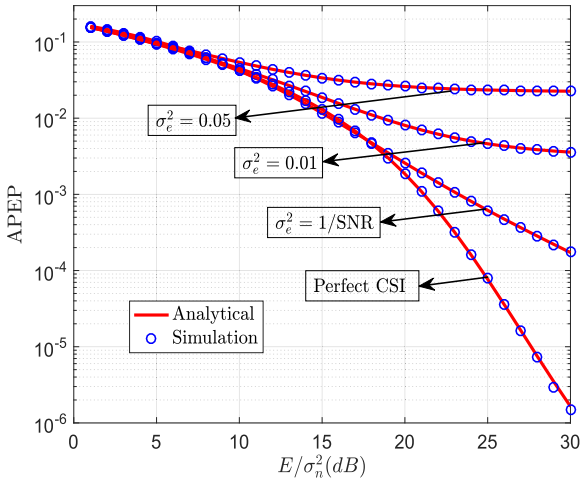

Fig. 3. APEP results of the proposed optimal MLD design for SM system under the effect of CSI impairment with perfect I/Q match ($q_B^2 = 0.01, r_B^2 = 0.09, K_B = 0.5, \rho_h = 0.9$).

First of all, the APEP results are given for the SM wireless communication system under the effect of only ICSI impairment assuming ideal hardware in Fig. 3. It is observed that even very small values of the channel estimation error have significant destructive impacts on the system performance. For instance, approximately a 7 dB power loss as well as an error floor are observed while $\mathrm{APEP} = 4\times10^{-3}$ for the estimation error value of just $\sigma_e^2 = 0.01$. On the other side, it can be noted that variable channel estimation ($\sigma_e^2 = 1/\mathrm{SNR}$) instead of constant values solves the error floor problem. However, this is not a complete solution since deterioration effect is not avoided, e.g., still $\sim$ 6 dB power loss is seen while $\mathrm{APEP} = 2\times10^{-4}$ compared to perfect CSI case.

The effect of IQI on the APEP performance can be analyzed by Fig. 4, which is given under the assumption of perfect CSI. In this figure, the results are presented for the varying values of amplitude imbalance between 0.5 to 1, and phase imbalance among 0° to 15°. Although it is clear that both amplitude and phase imbalance cause deterioration compared to the ideal case, i.e. $\xi_T = \xi_R = 1$ and $\phi_T = \phi_R = 0^\circ$, it is observed that an imbalance in phase has minor effects on the system performance, since changing $\phi_T = \phi_R = 10^\circ$ to $\phi_T = \phi_R = 15^\circ$ for fixed value of $\xi_T = \xi_R = 0.5$ provides almost the same results.

Fig. 5 is given to analyze the joint effect of IQI and ICSI on the APEP performance. It is observed that boosting the effect of estimation error by changing the variance of the error from $\sigma_e^2 = 0.01$ to $\sigma_e^2 = 0.03$ for the fixed values of $\xi_T = \xi_R = 0.9$ and $\phi_T = \phi_R = 5^\circ$, results in a remarkable signal distortion. Contrary to this, increasing the IQI effect by changing $\xi_T = \xi_R = 0.9$ and $\phi_T = \phi_R = 5^\circ$ to $\xi_T = \xi_R = 0.5$

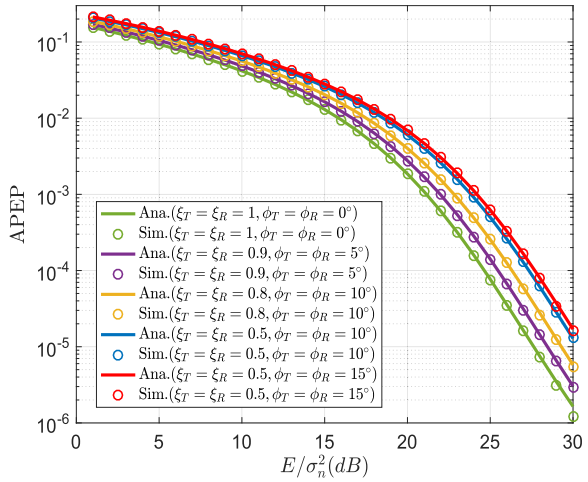

Fig. 4. APEP results of the proposed optimal MLD design for SM system under the effect of IQI with perfect CSI ($q_B^2 = 0.01, r_B^2 = 0.09, K_B = 0.5, \rho_h = 0.9$).

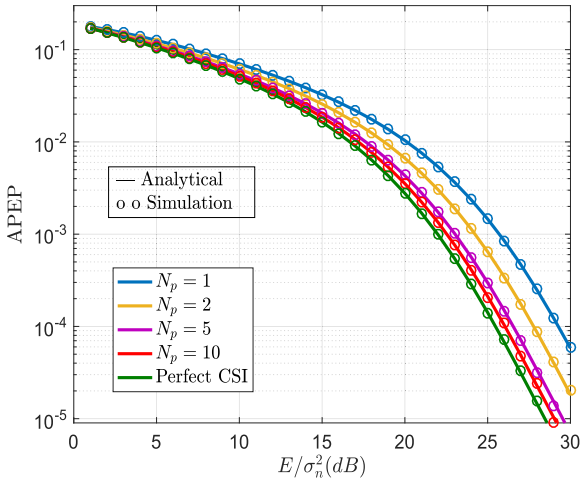

Fig. 6. APEP results of SM with CRLB under the joint effect of IQI and imperfect CSI ($q_B^2 = 0.01, r_B^2 = 0.09, K_B = 0.5, \rho_h = 0.9, \xi_T = \xi_R = 0.9$ and $\phi_T = \phi_R = 5°$).

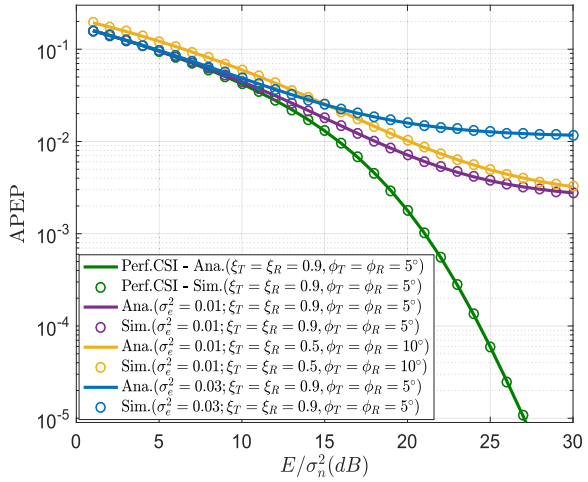

Fig. 5. APEP results of the proposed optimal MLD design for SM system under the joint effect of IQI and imperfect CSI ($q_B^2 = 0.01, r_B^2 = 0.09, K_B = 0.6, \rho_h = 0.9$).

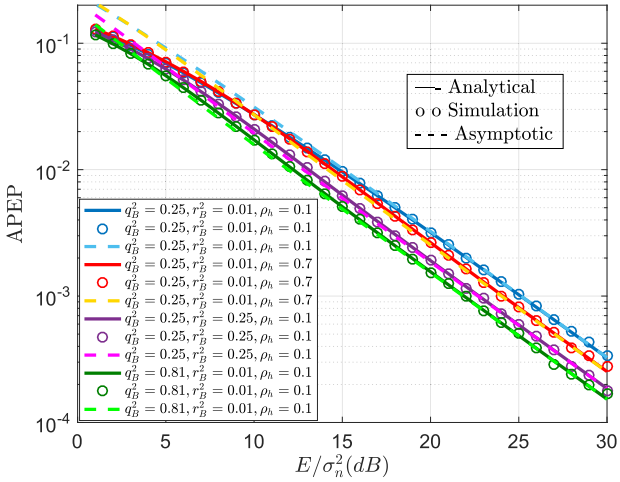

Fig. 7. APEP results of SM wireless system with CRLB under the joint effect of IQI and imperfect CSI ($K_B = 1, \xi_T = \xi_R = 0.9, \phi_T = \phi_R = 5°, N_P = 2$).

and $\phi_T = \phi_R = 10°$ for fixed σ_e^2 also impairs the system performance; however, this degradation impact is less than the one caused by the estimation error.

Considering both Figs. 3 and 5, it is easy to say that estimation at the Rx-side is very important for SM-MIMO systems over generalized Beckmann channels. Thus, in order to decrease the deterioration arising from estimation errors, CRLB, which calculates a lower bound for σ_e^2, is utilized for the proposed system. The positive effect of using CRLB is proven with Fig. 6, since the error floor observed for fixed values of σ_e^2 in Figs. 3 and 5, is eliminated. Moreover, considering this figure, it can also be demonstrated that increasing the number of pilot symbols used in CRLB improves the APEP results as well. For instance, using 10 pilot symbols instead of 1 provides ~ 3 dB gain in power when APEP $= 10^{-4}$.

The effect of the characteristic properties of the generalized Beckmann fading parameters on the system performance is clarified with Fig. 7. As seen from this figure, increasing the correlation between the real and imaginary parts of the channel coefficients by changing ρ_h from 0.1 to 0.7, provides 1 dB gain in power. The ascending imbalance between the mean ($r_B = 0.1$ to $r_B = 0.5$) and variance ($q_B^2 = 0.25$ to $q_B = 0.81$) values of the real and imaginary parts of the channel coefficients also gives approximately 2 dB and 3 dB better results. The effect of the parameter K_B, which stands for the ratio between the summation of the means and variances of I/Q parts of the channel coefficients, can be interpreted by comparing Figs. 4 and 5 for $\xi_T = \xi_R = 0.9, \phi_T = \phi_R = 5°$ case. Considering ~ 2 dB power gain provided with $K_B = 0.6$ in Fig. 5 as compared to $K_B = 0.5$ case in Fig. 4, it can be understood that increasing K_B improves the APEP performance as well.

Finally, Fig. 8 is given not only to show that the proposed design is applicable for higher order modulation schemes, i.e., higher data rates, but also to prove that the diversity gain is equal to the number of Rx antennas. Using $16-$QAM instead of $4-$QAM increases the data rate from 3 bps/Hz to 5 bps/Hz; however, it decreases the SNR around 3 dB for both

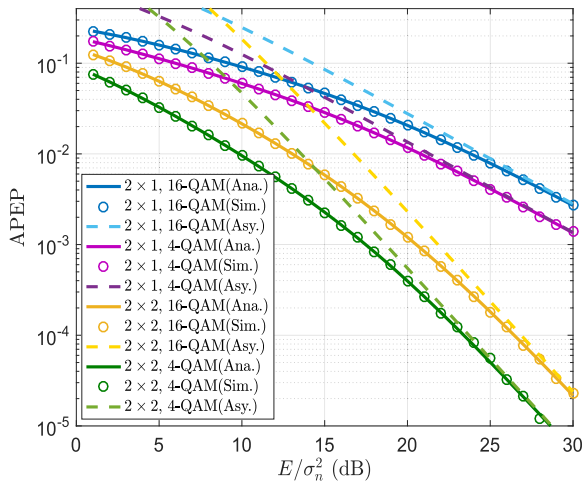

Fig. 8. APEP results of 2×1 and 2×2 SM wireless systems with CRLB in the presence of both IQI and imperfect CSI for different modulation schemes ($q_B^2 = 0.01, r_B^2 = 0.01, K_B = 0.5, \rho_h = 0.1, \xi_T = \xi_R = 0.9$ and $\phi_T = \phi_R = 5^\circ, N_P = 10$).

2×1 and 2×2 configurations. Considering APEP $= 10^{-2}$ case, 2×2 SM structure doubles the power of 2×1, which proves the comment on diversity gain. The accuracy of the asymptotic analysis could also be proved by considering Figs. 7 and 8 together, since the analytical and simulation results are in perfect agreement with the asymptotic results. During the simulations, it is assumed that $\sigma_I^2 + \sigma_Q^2 = 1$. Considering this case beside (3) and (4), the effect of the parameters K_B and Ω_B would be parallel.

VI. Conclusion

The destructive effects of IQI, which are highlighted in terms of SIR, as well as channel estimation error on the performance of SM-MIMO wireless communication system have been addressed via computer simulations and analytical derivations in this study. An upper-bound of the closed-form of APEP has been derived for the proposed optimal MLD method, and the performance results have been obtained over generalized Beckmann fading channels, which has been considered as the first time for SM-MIMO systems. The obtained results point out that both IQI and ICSI are major drawbacks for SM-MIMO systems, and the proposed optimal MLD design successfully mitigates the destructive effects of them. A further performance improvement has been achieved by utilizing CRLB for the channel estimation process. As increasing data rates cost more performance degradations, the effects of IQI has to be considered seriously while designing next-generation wireless systems. Future work can focus to the extention of the presented analysis to more challenging propagation environments and frequency-domain effects of IQI, while also extending the work towards cooperative MIMO systems offers an interesting topic for future studies.

Appendix A
CRLB for SM-MIMO System

The received signal at the Rx side, y_l, can be written in the form of:

$$y_l = y_l^I + j y_l^Q. \tag{44}$$

Expanding (10), y_l^Q and y_l^I can be obtained as follows, respectively:

$$\begin{aligned} y_l^Q &= \sqrt{E}[h_{l,i}^I(\tilde{x}_q^I K_c + \tilde{x}_q^Q K_d) + h_{l,i}^Q(\tilde{x}_q^I K_d - \tilde{x}_q^Q K_c)] \\ &\quad + K_c n_l^I + K_d n_l^Q \\ y_l^I &= \sqrt{E}(h_{l,i}^I \tilde{x}_q^I - h_{l,i}^Q \tilde{x}_q^Q) + n_l^I. \end{aligned} \tag{45}$$

Here, the noise parts of y_l^I and y_l^Q are given as $\eta^I = n_l^I$ and $\eta^Q = K_c n_l^I + K_d n_l^Q$ of which the variance values are calculated as $\sigma_{\eta^I}^2 = \sigma_n^2/2$ and $\sigma_{\eta^Q}^2 = (\xi_R^2 \sigma_n^2)/2$, respectively.

In light of this information, the joint PDF of y_l^I and y_l^Q is obtained as in (46), shown at the top of the next page. Considering this PDF, the likelihood function is also written as given in (47), shown at the top of the next page. In order to find the CRLB matrix, the log-likelihood function, which is necessary to get the values of $I_{(\boldsymbol{h}_i^I)}$, $I_{(\boldsymbol{h}_i^Q)}$ and $I_{(\boldsymbol{h}_i^I, \boldsymbol{h}_i^Q)}$ of FIM in (18), is achieved as (48), shown at the top of the next page, while the second derivative of $\ln(P_{\boldsymbol{y}}(\tilde{\boldsymbol{y}}; \boldsymbol{h}_i))$ is given in (49), shown at the top of the next page. Now, the value of $I_{(\boldsymbol{h}_i^I)}$ can be calculated by using the derivation in (49) from:

$$I_{(\boldsymbol{h}_i^I)} = -\mathbb{E}\left\{\frac{\partial^2(\ln(P_{\boldsymbol{y}}(\tilde{\boldsymbol{y}}; \boldsymbol{h}_i)))}{\partial (h_{l,i}^I)^2}\right\}. \tag{50}$$

Substituting (49) in (50) ends up with (19). Similarly, $I_{(\boldsymbol{h}_i^Q)}$ and $I_{(\boldsymbol{h}_i^I, \boldsymbol{h}_i^Q)}$, which is equal to $I_{(\boldsymbol{h}_i^Q, \boldsymbol{h}_i^I)}$, can be calculated by utilizing the derivations in (53) and (54), shown at the top of the next page, in the following expressions, respectively:

$$I_{(\boldsymbol{h}_i^Q)} = -\mathbb{E}\left\{\frac{\partial^2(\ln(P_{\boldsymbol{y}}(\tilde{\boldsymbol{y}}; \boldsymbol{h}_i)))}{\partial (h_{l,i}^Q)^2}\right\}, \tag{51}$$

$$I_{(\boldsymbol{h}_i^I, \boldsymbol{h}_i^Q)} = -\mathbb{E}\left\{\frac{\partial^2(\ln(P_{\boldsymbol{y}}(\tilde{\boldsymbol{y}}; \boldsymbol{h}_i)))}{\partial h_{l,i}^I \partial h_{l,i}^Q}\right\}. \tag{52}$$

Using these values in (22) gives the CRLB matrix.

Appendix B
MGF of Quadratic Form Correlated Noncentral Chi-Squared Distribution

Linear combination of two correlated noncentral chi-squared RVs with one degree of freedom, $\boldsymbol{\gamma}$, can be written in a quadratic form of Gaussian RVs as follows [56]:

$$\boldsymbol{\gamma} = \boldsymbol{\delta}^T \boldsymbol{A} \boldsymbol{\delta} = \sum_{j=1}^{2} \lambda_j (U_j + b_j)^2, \tag{55}$$

where U_j represents independently distributed standard normal variables and $\boldsymbol{\delta}^T = \begin{bmatrix}\zeta_1 & \zeta_2\end{bmatrix}$. λ_j are the eigenvalues of $\Sigma^{\frac{1}{2}} \boldsymbol{A} \Sigma^{\frac{1}{2}}$, where Σ is the covariance matrix of ζ_1 and ζ_2, and $\boldsymbol{A}$ is given as:

$$\boldsymbol{A} = \begin{bmatrix} \dfrac{\upsilon_1}{\sigma_{\tilde{n}_l^I}^2} & \dfrac{-\rho\sqrt{\upsilon_1 \upsilon_2}}{\sigma_{\tilde{n}_l^I} \sigma_{\tilde{n}_l^Q}} \\ \dfrac{-\rho\sqrt{\upsilon_1 \upsilon_2}}{\sigma_{\tilde{n}_l^I} \sigma_{\tilde{n}_l^Q}} & \dfrac{\upsilon_2}{\sigma_{\tilde{n}_l^Q}^2} \end{bmatrix}. \tag{56}$$

Additionally, in (48), $(b_1, b_2) \equiv \boldsymbol{b} = \boldsymbol{L}^T \boldsymbol{\Sigma}^{-\frac{1}{2}} \boldsymbol{\mu}$ is the reorganized mean vector where $(\mu_1, \mu_2) \equiv \boldsymbol{\mu}$ is the mean

$$f_{y_l}(y_l^I, y_l^Q) = \frac{1}{2\pi\sigma_{\eta^I}\sigma_{\eta^Q}\sqrt{1-\rho_\eta^2}} \times \exp\left[\frac{-1}{2(1-\rho_\eta^2)}\left(\frac{|y_l^I - \sqrt{E}(h_{l,i}^I\tilde{x}_q^I - h_{l,i}^Q\tilde{x}_q^Q)|^2}{\sigma_{\eta^I}^2} + \frac{|y_l^Q - \sqrt{E}[h_{l,i}^I(\tilde{x}_q^I K_c + \tilde{x}_q^Q K_d) + h_{l,i}^Q(\tilde{x}_q^I K_d - \tilde{x}_q^Q K_c)]|^2}{\sigma_{\eta^Q}^2} - \frac{2\rho_\eta[y_l^I - \sqrt{E}(h_{l,i}^I\tilde{x}_q^I - h_{l,i}^Q\tilde{x}_q^Q)]\{y_l^Q - \sqrt{E}[h_{l,i}^I(\tilde{x}_q^I K_c + \tilde{x}_q^Q K_d) + h_{l,i}^Q(\tilde{x}_q^I K_d - \tilde{x}_q^Q K_c)]\}}{\sigma_{\eta^I}\sigma_{\eta^Q}}\right)\right]. \quad (46)$$

$$P_{\boldsymbol{y}}(\tilde{\boldsymbol{y}}; \boldsymbol{h}_i) = \left(\frac{1}{2\pi\sigma_{\eta^I}\sigma_{\eta^Q}\sqrt{1-\rho_\eta^2}}\right)^{N_p} \times \exp\left[\frac{-1}{2(1-\rho_\eta^2)}\sum_{r=0}^{N_p-1}\left(\frac{|y_l^I - \sqrt{E}(h_{l,i}^I\tilde{x}_q^I - h_{l,i}^Q\tilde{x}_q^Q)|^2}{\sigma_{\eta^I}^2} + \frac{|y_l^Q - \sqrt{E}[h_{l,i}^I(\tilde{x}_q^I K_c + \tilde{x}_q^Q K_d) + h_{l,i}^Q(\tilde{x}_q^I K_d - \tilde{x}_q^Q K_c)]|^2}{\sigma_{\eta^Q}^2} - \frac{2\rho_\eta[y_l^I - \sqrt{E}(h_{l,i}^I\tilde{x}_q^I - h_{l,i}^Q\tilde{x}_q^Q)]\{y_l^Q - \sqrt{E}[h_{l,i}^I(\tilde{x}_q^I K_c + \tilde{x}_q^Q K_d) + h_{l,i}^Q(\tilde{x}_q^I K_d - \tilde{x}_q^Q K_c)]\}}{\sigma_{\eta^I}\sigma_{\eta^Q}}\right)\right]. \quad (47)$$

$$\ln(P_{\boldsymbol{y}}(\tilde{\boldsymbol{y}}; \boldsymbol{h}_i)) = -N_p\ln(2\pi\sigma_{\eta^I}\sigma_{\eta^Q}\sqrt{1-\rho_\eta^2}) - \frac{N_p}{2(1-\rho_\eta^2)} \times \left(\frac{|y_l^I - \sqrt{E}(h_{l,i}^I\tilde{x}_q^I - h_{l,i}^Q\tilde{x}_q^Q)|^2}{\sigma_{\eta^I}^2} + \frac{|y_l^Q - \sqrt{E}[h_{l,i}^I(\tilde{x}_q^I K_c + \tilde{x}_q^Q K_d) + h_{l,i}^Q(\tilde{x}_q^I K_d - \tilde{x}_q^Q K_c)]|^2}{\sigma_{\eta^Q}^2} - \frac{2\rho_\eta[y_l^I - \sqrt{E}(h_{l,i}^I\tilde{x}_q^I - h_{l,i}^Q\tilde{x}_q^Q)]\{y_l^Q - \sqrt{E}[h_{l,i}^I(\tilde{x}_q^I K_c + \tilde{x}_q^Q K_d) + h_{l,i}^Q(\tilde{x}_q^I K_d - \tilde{x}_q^Q K_c)]\}}{\sigma_{\eta^I}\sigma_{\eta^Q}}\right). \quad (48)$$

$$\frac{\partial^2(\ln(P_{\boldsymbol{y}}(\tilde{\boldsymbol{y}}; \boldsymbol{h}_i)))}{\partial(h_{l,i}^I)^2} = \frac{-N_pE}{1-\rho_\eta^2} \times \left(\frac{(\tilde{x}_q^I)^2}{\sigma_{\eta^I}^2} + \frac{(\tilde{x}_q^I K_c + \tilde{x}_q^Q K_d)^2}{\sigma_{\eta^Q}^2} - \frac{2\rho_\eta\tilde{x}_q^I(\tilde{x}_q^I K_c + \tilde{x}_q^Q K_d)}{\sigma_{\eta^I}\sigma_{\eta^Q}}\right) \quad (49)$$

$$\frac{\partial^2(\ln(P_{\boldsymbol{y}}(\tilde{\boldsymbol{y}}; \boldsymbol{h}_i)))}{\partial(h_{l,i}^Q)^2} = \frac{-N_pE}{1-\rho_\eta^2} \times \left(\frac{(\tilde{x}_q^Q)^2}{\sigma_{\eta^I}^2} + \frac{(\tilde{x}_q^I K_d - \tilde{x}_q^Q K_c)^2}{\sigma_{\eta^Q}^2} + \frac{2\rho_\eta\tilde{x}_q^Q(\tilde{x}_q^I K_d - \tilde{x}_q^Q K_c)}{\sigma_{\eta^I}\sigma_{\eta^Q}}\right). \quad (53)$$

$$\frac{\partial^2(\ln(P_{\boldsymbol{y}}(\tilde{\boldsymbol{y}}; \boldsymbol{h}_i)))}{\partial h_{l,i}^I\partial h_{l,i}^Q} = \frac{-N_pE}{1-\rho_\eta^2} \times \left(\frac{-\tilde{x}_q^I\tilde{x}_q^Q}{\sigma_{\eta^I}^2} + \frac{(\tilde{x}_q^I K_d - \tilde{x}_q^Q K_c)(\tilde{x}_q^I K_c + \tilde{x}_q^Q K_d)}{\sigma_{\eta^Q}^2} + \frac{\rho_\eta(\tilde{x}_q^Q(\tilde{x}_q^I K_c + \tilde{x}_q^Q K_d) + \tilde{x}_q^I(\tilde{x}_q^I K_d - \tilde{x}_q^Q K_c))}{\sigma_{\eta^I}\sigma_{\eta^Q}}\right) \quad (54)$$

vector of $\boldsymbol{\zeta}_1$ and $\boldsymbol{\zeta}_2$, and $\boldsymbol{L}$ is the eigenvector that is calculated by using λ_1 and λ_2.

The moment generation function (MGF) of $\boldsymbol{\gamma}$ can be given by the following expression [56]:

$$M_\gamma(t) = \prod_{j=1}^{s}(1-2t\lambda_j)^{-\frac{1}{2}}\exp\left\{\sum_{j=1}^{s}\frac{b_j^2 t\lambda_j}{1-2t\lambda_j}\right\}, \quad (57)$$

where s is the number of correlated noncentral chi-squared variables. This equation reaches to (36) for SM-MIMO wireless communication systems under the assumption of independent channels.

REFERENCES

[1] K. Pretz. (Mar. 2017). *5G: The Future of Communications Networks*. [Online]. Available: https://spectrum.ieee.org/the-institute/ieee-products-services/5g-the-future-of-communications-networks

[2] International Telecommunications Union (ITU), "Minimum requirements related to technical performance for IMT-2020 radio interface(s)," Geneva, Switzerland, Tech. Rep. M.2410-0, Nov. 2017. [Online]. Available: https://www.itu.int/pub/R-REP-M.2410-2017

[3] E. Basar, M. Wen, R. Mesleh, M. Di Renzo, Y. Xiao, and H. Haas, "Index modulation techniques for next-generation wireless networks," *IEEE Access*, vol. 5, pp. 16693–16746, 2017.

[4] E. Basar, "Index modulation techniques for 5G wireless networks," *IEEE Commun. Mag.*, vol. 54, no. 7, pp. 168–175, Jul. 2016.

[5] Y. Chau and S.-H. Yu, "Space modulation on wireless fading channels," in *Proc. IEEE 54th Veh. Technol. Conf. (VTC Fall)*, vol. 3, Oct. 2001, pp. 1668–1671.

[6] M. D. Renzo and H. Haas, "Space shift keying (SSK—) MIMO over correlated Rician fading channels: Performance analysis and a new method for transmit-diversity," *IEEE Trans. Commun.*, vol. 59, no. 1, pp. 116–129, Jan. 2011.

[7] R. Y. Mesleh *et al.*, "Spatial modulation," *IEEE Trans. Veh. Technol.*, vol. 57, no. 4, pp. 2228–2241, Jul. 2008.

[8] L. Xiao, L. Greenstein, N. Mandayam, and W. Trappe, "Using the physical layer for wireless authentication in time-variant channels," *IEEE Trans. Wireless Commun.*, vol. 7, no. 7, pp. 2571–2579, Jul. 2008.

[9] E. Başar, U. Aygolu, E. Panayirci, and H. V. Poor, "Space-time block coded spatial modulation," *IEEE Trans. Commun.*, vol. 59, no. 3, pp. 823–832, Mar. 2011.

[10] T. Handte, A. Müller, and J. Speidel, "BER analysis and optimization of generalized spatial modulation in correlated fading channels," in *Proc. IEEE 70th Veh. Technol. Conf. Fall*, Sep. 2009, pp. 1–5.

[11] M. Di Renzo, H. Haas, A. Ghrayeb, S. Sugiura, and L. Hanzo, "Spatial modulation for generalized MIMO: Challenges, opportunities, and implementation," *Proc. IEEE*, vol. 102, no. 1, pp. 56–103, Jan. 2014.

[12] P. Yang, M. Di Renzo, Y. Xiao, S. Li, and L. Hanzo, "Design guidelines for spatial modulation," *IEEE Commun. Surveys Tuts.*, vol. 17, no. 1, pp. 6–26, 1st Quart., 2015.

[13] Y. Xiao, L. Xiao, L. Dan, and X. Lei, "Spatial modulation for 5G MIMO communications," in *Proc. 19th Int. Conf. Digit. Signal Process.*, Aug. 2014, pp. 847–851.

[14] E. Basar, "Spatial modulation techniques for 5G wireless networks," in *Proc. 24th Signal Process. Commun. Appl. Conf. (SIU)*, May 2016, pp. 777–780.

[15] J. Jeganathan, A. Ghrayeb, and L. Szczecinski, "Spatial modulation: Optimal detection and performance analysis," *IEEE Commun. Lett.*, vol. 12, no. 8, pp. 545–547, Aug. 2008.

[16] M. Koca and H. Sari, "Performance analysis of spatial modulation over correlated fading channels," in *Proc. IEEE Veh. Technol. Conf. (VTC Fall)*, Sep. 2012, pp. 1–5.

[17] A. Younis, *Spatial Modulation: Theory to Practice*. Edinburgh, U.K.: Univ. of Edinburgh, 2014. [Online]. Available: https://books.google.com.tr/books?id=JIvcoQEACAAJ

[18] M. Di Renzo and H. Haas, "Bit error probability of SM-MIMO over generalized fading channels," *IEEE Trans. Veh. Technol.*, vol. 61, no. 3, pp. 1124–1144, Mar. 2012.

[19] E. Basar, U. Aygolu, E. Panayirci, and H. V. Poor, "Performance of spatial modulation in the presence of channel estimation errors," *IEEE Commun. Lett.*, vol. 16, no. 2, pp. 176–179, Feb. 2012.

[20] S. S. Ikki and R. Mesleh, "A general framework for performance analysis of space shift keying (SSK) modulation in the presence of Gaussian imperfect estimations," *IEEE Commun. Lett.*, vol. 16, no. 2, pp. 228–230, Feb. 2012.

[21] O. S. Badarneh, R. Mesleh, S. S. Ikki, and H. M. Aggoune, "Performance analysis of space modulation techniques over alpha–μ fading channels with imperfect channel estimation," in *Proc. IEEE 80th Veh. Technol. Conf. (VTC-Fall)*, Sep. 2014, pp. 1–5.

[22] O. S. Badarneh and R. Mesleh, " On the performance of space modulations over κ-μ fading channels with imperfect CSI," in *Proc. IEEE Wireless Commun. Netw. Conf. (WCNC)*, Mar. 2015, pp. 189–194.

[23] E. Bjornson, M. Matthaiou, and M. Debbah, "A new look at dual-hop relaying: Performance limits with hardware impairments," *IEEE Trans. Commun.*, vol. 61, no. 11, pp. 4512–4525, Nov. 2013.

[24] A. G. Helmy, M. Di Renzo, and N. Al-Dhahir, "On the robustness of spatial modulation to I/Q imbalance," *IEEE Commun. Lett.*, vol. 21, no. 7, pp. 1485–1488, Jul. 2017.

[25] A. E. Canbilen, S. S. Ikki, E. Basar, S. S. Gultekin, and I. Develi, "Impact of I/Q imbalance on amplify-and-forward relaying: Optimal detector design and error performance," *IEEE Trans. Commun.*, vol. 67, no. 5, pp. 3154–3166, May 2019.

[26] M. M. Alsmadi, A. E. Canbilen, N. Abu Ali, S. S. Ikki, and E. Basar, "Cognitive networks in the presence of I/Q imbalance and imperfect CSI: Receiver design and performance analysis," *IEEE Access*, vol. 7, pp. 49765–49777, 2019.

[27] R. Mesleh, S. S. Ikki, and F. S. Almehmadi, "Impact of IQ imbalance on the performance of QSM multiple-input–multiple-output system," *IET Commun.*, vol. 10, no. 17, pp. 2391–2395, Nov. 2016.

[28] A. E. Canbilen, M. M. Alsmadi, E. Basar, S. S. Ikki, S. S. Gultekin, and I. Develi, "Spatial modulation in the presence of I/Q imbalance: Optimal detector & performance analysis," *IEEE Commun. Lett.*, vol. 22, no. 8, pp. 1572–1575, Aug. 2018.

[29] A. Afana and S. Ikki, "Analytical framework for space shift keying MIMO systems with hardware impairments and co-channel interference," *IEEE Commun. Lett.*, vol. 21, no. 3, pp. 488–491, Mar. 2017.

[30] L. Berriche, K. Abed-Meraim, and J. Belfiore, "Cramer–Rao bounds for MIMO channel estimation," in *Proc. IEEE Int. Conf. Acoust., Speech, Signal Process.*, vol. 4, May 2004, pp. 397–400.

[31] A. Afana, N. Abu-Ali, and S. Ikki, "On the joint impact of hardware and channel imperfections on cognitive spatial modulation MIMO systems: Cramer–Rao bound approach," *IEEE Syst. J.*, vol. 13, no. 2, pp. 1250–1261, Jun. 2019.

[32] F. S. Al-Qahtani, S. Ikki, M. Di Renzo, and H. Alnuweiri, "Performance analysis of space shift keying modulation with imperfect estimation in the presence of co-channel interference," *IEEE Commun. Lett.*, vol. 18, no. 9, pp. 1587–1590, Sep. 2014.

[33] M. Di Renzo, D. De Leonardis, F. Graziosi, and H. Haas, "Space shift keying (SSK—) MIMO with practical channel estimates," *IEEE Trans. Commun.*, vol. 60, no. 4, pp. 998–1012, Apr. 2012.

[34] E. Soujeri and G. Kaddoum, "Performance comparison of spatial modulation detectors under channel impairments," in *Proc. IEEE Int. Conf. Ubiquitous Wireless Broadband (ICUWB)*, Oct. 2015, pp. 1–5.

[35] H. Al-Quwaiee, H.-C. Yang, and M.-S. Alouini, "On the asymptotic ergodic capacity of FSO links with generalized pointing error model," in *Proc. IEEE Int. Conf. Commun. (ICC)*, Jun. 2015, pp. 5072–5077.

[36] B. Zhu, Z. Zeng, J. Cheng, and N. C. Beaulieu, "On the distribution function of the generalized Beckmann random variable and its applications in communications," *IEEE Trans. Commun.*, vol. 66, no. 5, pp. 2235–2250, May 2018.

[37] J. P. Pena-Martin, J. M. Romero-Jerez, and F. J. Lopez-Martinez, "Generalized MGF of Beckmann fading with applications to wireless communications performance analysis," *IEEE Trans. Commun.*, vol. 65, no. 9, pp. 3933–3943, Sep. 2017.

[38] F. Yang, J. Cheng, and T. A. Tsiftsis, "Free-space optical communication with nonzero boresight pointing errors," *IEEE Trans. Commun.*, vol. 62, no. 2, pp. 713–725, Feb. 2014.

[39] J. P. Pena-Martin, J. M. Romero-Jerez, and F. J. Lopez-Martinez, "Analysis of energy detection of unknown signals under Beckmann fading channels," in *Proc. IEEE 85th Veh. Technol. Conf. (VTC Spring)*, Jun. 2017, pp. 1–6.

[40] B. Zhu, J. Cheng, N. Al-Dhahir, and L. Wu, "Asymptotic analysis and tight performance bounds of diversity receptions over Beckmann fading channels with arbitrary correlation," *IEEE Trans. Commun.*, vol. 64, no. 5, pp. 2220–2234, May 2016.

[41] A. Gouissem, R. Hamila, and M. O. Hasna, "Outage performance of cooperative systems under IQ imbalance," *IEEE Trans. Commun.*, vol. 62, no. 5, pp. 1480–1489, May 2014.

[42] V. Aalo, G. Efthymoglou, and C. Chayawan, "On the envelope and phase distributions for correlated Gaussian quadratures," *IEEE Commun. Lett.*, vol. 11, no. 12, pp. 985–987, Dec. 2007.

[43] Y. Zou, M. Valkama, and M. Renfors, "Digital compensation of I/Q imbalance effects in space-time coded transmit diversity systems," *IEEE Trans. Signal Process.*, vol. 56, no. 6, pp. 2496–2508, Jun. 2008.

[44] J. Li, M. Matthaiou, and T. Svensson, "I/Q imbalance in AF dual-hop relaying: Performance analysis in Nakagami-m fading," *IEEE Trans. Commun.*, vol. 62, no. 3, pp. 836–847, Mar. 2014.

[45] M. Valkama, M. Renfors, and V. Koivunen, "Advanced methods for I/Q imbalance compensation in communication receivers," *IEEE Trans. Signal Process.*, vol. 49, no. 10, pp. 2335–2344, Oct. 2001.

[46] T. Schenk, *RF Imperfections in High-Rate Wireless Systems: Impact and Digital Compensation*. Dordrecht, The Netherlands: Springer, Jan. 2008.

[47] D. L. N. S. Inti, "Time-varying frequency selective IQ imbalance estimation and compensation," Ph.D. dissertation, Virginia Polytech. Inst. State Univ., Blacksburg, VA, USA, 2017.

[48] R. Mesleh and O. S. Badarneh, "Quadrature spatial modulation in correlated $\eta-\mu$ fading channels with imperfect channel state information," in *Proc. Int. Conf. Wireless Commun., Signal Process. Netw. (WiSPNET)*, Mar. 2017, pp. 887–892.

[49] A. Afana, T. M. N. Ngatched, and O. A. Dobre, "Spatial modulation in MIMO limited-feedback spectrum-sharing systems with mutual interference and channel estimation errors," *IEEE Commun. Lett.*, vol. 19, no. 10, pp. 1754–1757, Oct. 2015.

[50] A. Afana, T. M. N. Ngatched, O. A. Dobre, and S. Ikki, "Spatial modulation in MIMO spectrum-sharing systems with imperfect channel estimation and multiple primary users," in *Proc. IEEE Global Commun. Conf. (GLOBECOM)*, Dec. 2015, pp. 1–5.

[51] A. Afana, I. A. Mahady, and S. Ikki, "Quadrature spatial modulation in MIMO cognitive radio systems with imperfect channel estimation and limited feedback," *IEEE Trans. Commun.*, vol. 65, no. 3, pp. 981–991, Mar. 2017.

[52] J. M. Romero-Jerez and F. J. Lopez-Martinez, "On the distribution of the squared norm of non-circular complex Gaussian random variables with applications," in *Proc. IEEE Int. Symp. Inf. Theory (ISIT)*, Jun. 2015, pp. 341–345.

[53] A. Ly, M. Marsman, J. Verhagen, R. P. Grasman, and E.-J. Wagenmakers, "A tutorial on Fisher information," *J. Math. Psychol.*, vol. 80, pp. 40–55, Oct. 2017.

[54] S. Javed, O. Amin, S. S. Ikki, and M.-S. Alouini, "Impact of improper Gaussian signaling on hardware impaired systems," in *Proc. IEEE Int. Conf. Commun. (ICC)*, May 2017, pp. 1–6.
[55] A. S. Aghaei, K. N. Plataniotis, and S. Pasupathy, "Maximum likelihood binary detection in improper complex Gaussian noise," in *Proc. IEEE Int. Conf. Acoust., Speech Signal Process.*, Mar. 2008, pp. 3209–3212.
[56] B. Baldessari, "The distribution of a quadratic form of normal random variables," *Ann. Math. Statist.*, vol. 38, no. 6, pp. 1700–1704, Dec. 1967, doi: 10.1214/aoms/1177698604.
[57] M. K. Simon and M.-S. Alouini, *Digital Communication over Fading Channels*, 2nd ed. Hoboken, NJ, USA: Wiley, 2004.
[58] I. S. Gradshteyn and I. M. Ryzhik, *Table of Integrals, Series, and Products*, 7th ed. Amsterdam, The Netherlands: Elsevier, 2007.
[59] G. Andrews, R. Askey, and R. Roy, *Encyclopedia of Mathematics and its Applications 71: Special Functions*. Cambridge, U.K.: Cambridge Univ. Press, 1999.
[60] G. B. Arfken and H. J. Weber, *Mathematical Methods for Physicists*, 6th ed. Amsterdam, The Netherlands: Elsevier, 2005.

Ayse Elif Canbilen received the B.S. and M.S. degrees from Selçuk University, Turkey, in 2012 and 2015, respectively, and the Ph.D. degree from Konya Technical University, Turkey, in 2019, all in electrical and electronics engineering. From 2017 to 2018, she was with the Department of Electrical Engineering, Lakehead University, Thunder Bay, ON, Canada, as a Visitor Researcher. She is currently a Research Assistant with the Department of Electrical and Electronics Engineering, Konya Technical University. Her primary research interests include MIMO systems, spatial modulation techniques, cooperative communications, cognitive radio systems, and reconfigurable intelligent surfaces. She has been serving as a Reviewer for the IEEE TRANSACTIONS ON COMMUNICATIONS, the IEEE TRANSACTIONS ON WIRELESS COMMUNICATIONS, the IEEE TRANSACTIONS ON VEHICULAR TECHNOLOGY, the IEEE COMMUNICATIONS LETTERS, and IEEE ACCESS.

Salama Said Ikki (Senior Member, IEEE) received the B.S. degree from Al-Isra University, Amman, Jordan, in 1996, the M.Sc. degree from the Arab Academy for Science and Technology and Maritime Transport, Alexandria, Egypt, in 2002, and the Ph.D. degree from the Memorial University of Newfoundland, St. John's, in 2009, all in electrical engineering. He was a Research Assistant with INRS, University of Quebec, Montreal, from 2010 to 2012, and a Post-Doctoral Fellow with the University of Waterloo, Waterloo, ON, Canada, from 2009 to 2010. He is currently an Associate Professor in wireless communications with the Department of Electrical Engineering, Lakehead University. He has authored or coauthored more than 100 articles in peer-reviewed IEEE international journals and conferences with more than 3 500 citations and has a current H-index of 30. He has been carrying out research in communications and signal processing for over 10 years. He was a recipient of the Best Paper Award published in the *EURASIP Journal on Advances in Signal Processing*, the IEEE COMMUNICATIONS LETTERS and the IEEE WIRELESS COMMUNICATIONS LETTERS Exemplary Reviewer Certificate in 2012, and the Top Reviewer Certificate from the IEEE TRANSACTIONS ON VEHICULAR TECHNOLOGY in 2015. He serves on the Editorial Board of the IEEE COMMUNICATIONS LETTERS and the *IET Communications Proceeding*. He is widely recognized as an expert in the field of wireless communications.

Ertugrul Basar (Senior Member, IEEE) received the B.S. degree (Hons.) from Istanbul University, Turkey, in 2007, and the M.S. and Ph.D. degrees from Istanbul Technical University, Turkey, in 2009 and 2013, respectively. He is currently an Associate Professor with the Department of Electrical and Electronics Engineering, Koç University, Istanbul, Turkey, and also the Director of the Communications Research and Innovation Laboratory (CoreLab). His primary research interests include MIMO systems, index modulation, waveform design, visible light communications, and signal processing for communications.

Recent recognition of his research include the Science Academy (Turkey) Young Scientists (BAGEP) Award in 2018, the Mustafa Parlar Foundation Research Encouragement Award in 2018, the Turkish Academy of Sciences Outstanding Young Scientist (TUBA-GEBIP) Award in 2017, and the first-ever IEEE Turkey Research Encouragement Award in 2017. He currently serves as an Editor for the IEEE TRANSACTIONS ON COMMUNICATIONS and *Physical Communication* (Elsevier), and as an Associate Editor of the IEEE COMMUNICATIONS LETTERS. He served as an Associate Editor for IEEE ACCESS from 2016 to 2018.

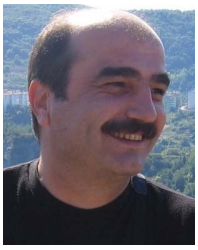

Seyfettin Sinan Gultekin received the B.S. and M.S. degrees from Erciyes University, Turkey, in 1988, and 1992, respectively, and the Ph.D. degree from Selçuk University in 2002. He was a Research Assistant, an Instructor, and then was an Assistant Professor with the Department of Electrical and Electronics Engineering, Selçuk University, Konya, Turkey, from 1989 to 1994, from 1994 to 2009, and from 2009 to 2018. He is currently an Associate Professor with the Department of Electrical and Electronics Engineering, Konya Technical University, Konya, Turkey. He teaches lectures on microwave, antenna, communications and engineering mathematics. His current research areas include microstrip antennas for wearable and biomedical applications, and optimization of microstrip antenna parameters. He served as a Local Organizing Committee Member for the International Union of Radio Science (URSI) Turkey Conference in 2018.

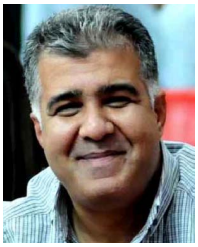

Ibrahim Develi received the B.S., M.S., and Ph.D. degrees from Erciyes University, Turkey, in 1995, 1997, and 2003, respectively. From 1995 to 2003, he was a Research Assistant with the Department of Electronics Engineering, Erciyes University, where he is currently a Professor. He teaches courses in wireless communications, and his current research interests are in cooperative communications, MIMO systems, spread spectrum communications, multiuser communications, wireless networks, and the applications of neural networks to multiuser communication systems. He has been a member of the TPC for a large number of major international conferences, such as IEEE ICC, IEEE GLOBECOM, IEEE BROADNETS, IEEE RWS, and IEEE WCNC. He currently serves as an Associate Editor for the *EURASIP Journal on Wireless Communications and Networking*. He is also on the Editorial Board of the *International Journal of Mobile Communications*.